NON-LINEAR INSTABILITIES
IN THIN FILMS
UNDERGOING PHASE CHANGE

A thesis submitted

in partial fulfilment of the requirements

for the degree of

Master of Technology

by

RAMAN

to the

DEPARTMENT OF CHEMICAL ENGINEERING
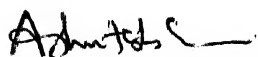
INDIAN INSTITUTE OF TECHNOLOGY, KANPUR

March, 1996

CHE-1996-M-RAM-NON

CERTIFICATE

Certified that the work contained in the thesis titled "Non-linear Instabilities in Thin Films Undergoing Phase Change ", by "RAMAN", has been carried out under my supervision and that this work has not been submitted elsewhere for a degree.
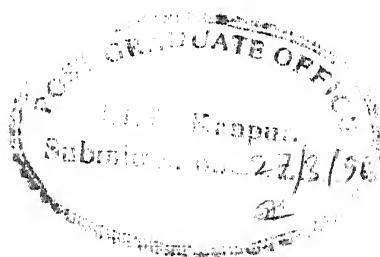
(Dr. Ashutosh Sharma)

Department of Chemical Engineering,

Indian Institute of Technology,

March 1996, Kanpur.

ABSTRACT

Thin liquid films when perturbed, either go to rupture or obtain an equilibrium configuration due to interfacial instabilities combined with evaporation (or condensation). This behaviour is studied using a continuum approach (Navier-Stokes eqation modified for intermolecular interactions). The dynamics is studied by numerical simulations of the non-linear partial differential evolution equation. Born repulsion is also incorporated to study the dynamics of the film even after rupture. The process of formation of nano-drops starting with a uniform thin film is studied. Usually hydrodynamic instabilities evolve on a short time scale, which first lead to a (quasi) mechanically stable structure. Evaporation becomes significant at longer times.

This technique is further applied to study the generation of critical nucleii under heterogeneous nucleation and the energy associated with these. An attempt is made to create the critical nucleii having minimum energy associted with them. Since critical nucleii are very small ($\sim$ 1 nm), the finite size effects including excess intermolecular interactions cannot be ignored as is done in classical theory of heterogeneous nucleation. Our results show that the energy barrier for nucleation may be many orders smaller than the predictions of the classical theory, which implies much faster rates of nucleation.

I dedicate this work to the lady whose love, sacrifices, ambitions, courage, patience and painstaking efforts have made me able to stand where I am.

DEDICATED

TO MY

MOTHER

ACKNOWLEDGEMENTS

Contents

List of Tables

List of Figures

Nomenclature

p_v	partial vapour pressure
p_o	saturation vapour pressure
R	universal gas constant
h	dimensional film thickness
h_o	dimensional mean film thickness (chapter 2)
	height of the drop (chapter 3 and 4)
h_e	equilibrium film thickness
S	spreading coefficient
S^{LW}	apolar component of spreading coefficint
S^P	polar component of spreading coefficint
G	free energy per unit area of intermolecular interactions
A	non-dimensional Hamaker constant
k	wave number of perturbation
k_m	dominant wave number of perturbation
$\dot{m}$	mass loss (or gain) due to evaporation (or condensation)
M	non-dimensional mass loss (or gain)
d_o	dimensional distance of minimum separation between atoms
d	non-dimensional distance of minimum separation between atoms
l_o	height at which bare surface is assumed
M_w	molecular weight of film liquid
$\overline{V}_L$	specific volume of film liquid
H	non-dimensional film thickness
X	axial co-ordinate
T	non-dimensional time
r_c	radius of curvature
c	a parameter (chapter 2)
	a constant (chapter 4)

Greek Symbols

ω	growth rate of initial perturbation
ϕ	potential due to intermolecular interactions
Φ	non-dimensional potential due to intermolecular interactions
ρ	density of liquid
ρ_v	density of vapour phase
ν	kinematic viscosity of film liquid
ϵ	amplitude of initial perturbation
λ	dimensional debye length of polar forces
σ	surface tension of the liquid
α	accommodation coefficient

Chapter 1

Introduction And Literature Survey

Thin liquid films are those which are thin enough so that their thermodynamic and transport behaviour depend on the film thickness. These films are in the range of 10 - 1000 Å. The interfacial hydrodynamics of these films subjected to various kinds of instabilities (long and short range intermolecular interactions, Marangoni flow, thermocapillarity effects, Rayleigh-Taylor instabilities etc.) is governed by all these forces. Their stability analysis gives the kinetics of deformation and equilibrium configurations.

Thin films are encountered in a lot of industrial applications, e.g. rupture of foams and soap bubbles, coalescence of drops or emulsions, enhanced oil recovery, froth floatation, wetting of surfaces, heterogeneous nucleation and in biomedical applications (e.g. cell adhesion to substrates, tear film rupture etc.).

Nucleation comes into picture in the formation of a new phase [1]. Small clusters of molecules form and these grow by accretion to the point of becoming recognizable droplets or crystals that may finally coalesce or grow to give massive amounts of new phase. For very pure substances nucleation does not take place easily because of the extra surface energy of small clusters. In the presence of a foreign material (e.g. a solid surface), the tendency of a liquid having contact angle less than 180^0 is to wet the surface. This wettability of the liquid on the solid makes it easier to attatch to the solid and ,therfore, a smaller nucleus can grow. It reduces the energy required to create the critical nucleus.

The linear theory for falling films was first studied by Yih [2] and Benjamin [3].

Benny [4] and Atherton and Homsy [5] derived the non-linear evolution eqation at the film interface. Scheludko [6] and Vrij [7] studied the effect of van der Waals interactions and estimated a critical film thickness at which a non-thinning film becomes unstable and ruptures. Ruckenstein and Jain [8] modelled the liquid as a Navier Stokes continuum modified by van der Waals interactions. They used the lubrication approximation to obtain the dynamic linear stability results. Williams and Davis [9] adapted the long wave reduction procedure and derived the non-linear partial differential equation describing the evolution of film interface. Teletzke, Davis and Scriven [10] put forward a theory of wetting of solids by liquids accounting for capillary pressure gradient, gravitational potential gradient, surface tension gradient and disjoining pressure gradient. Stability of free films was studied by Sharma, Kishore and Salaniwal [11].

The effect of interfacial mass transport on the stability and flow of thin filmswas studied by Wayner [12] and an expression for interfacial mass flux was obtained. Similar expressions were obtained by Sharma [13].For evaporating films vapour recoil instabilitis were studied by Hickman [14] and Palmer and Maheshri [15]. Bankoff [16] studied the evaporating film assuming the interface to be always at saturation temperature. Burelbach, Bankoff and Davis [17] considered an evaporating film with heat transfer and derived a model for evaporation. They predicted complete dryout (film rupture) for positive Hamaker constant. Sharma and Ruckenstein [18] employed a non-linear analytical theory which was in agreement with the results of Burelbach et al.[17]. Analytical findings of Sharma and Ruckenstein [19]-[20] show discrepancies in rupture times as computed from linear and non-linear theories. The effect of acid-base forces in polar systems has also been studied [21]. The role of intermolecular interactions in coexistence of drops with thin films was studied by Sharma [22] and Sharma and Jameel [23].

In the first part of the present work, Born repulsion is incorporated to the intermolecular interactions to study the films even after rupture. In the second part this approach is applied to study the generation of critical nucleii under heterogeneous nucleation and energy associated with these.

Chapter 2

Evaporating-Condensing Thin Liquid Films

2.1   Introduction

The evaporation from or condensation to a thin liquid film depends not only on the relative saturation in the vapour atmosphere but also on hydrodynamic conditions of the film viz. thickness of the film and its intermolecular interactions with the surface supporting it. In this chapter we have shown the effect of these instabilities on the evolution of the film. The effect of Born repulsion is also studied. The instability due to vapour recoil was found to exert negligible effect on the behaviour of the film [18]. Therefore, these are not considered.

2.2   Formulation Of Problem

2.2.1   Dimensional Equations

The time evolution eqn. (non-linear hydrodynamic eqn. neglecting the vapour recoil instabilities) for a thin liquid film (evaporating or condensing) resting on a plane surface (fig. 1) is obtained from Navier-Stokes equation [24] neglecting gravitational effects and considering intermolecular interactions. The equations are solved in two dimensions only assuming the film to be infinite in the third dimension. The equation is given [18], [13] as-

$$h_t + \frac{\dot{m}}{\rho} - \frac{1}{3\mu} \left[h^3 \left(p + \phi \right)_x \right]_x = 0 \qquad (2.1)$$

where p is the pressure as given by Young-Laplace equation for capillarity-

$$p - p_v = \frac{-\sigma h_{xx}}{(1 + h_x^2)^{3/2}} \tag{2.2}$$

ϕ is the force due to intermolecular interactions given as-

$$\phi = \frac{\partial G}{\partial h} = -2S^{LW}\frac{d_o^2}{h^3} - \frac{S^P}{\lambda}\exp\left(\frac{d_o - h}{\lambda}\right) \tag{2.3}$$

S^{LW} and S^P are the apolar and polar components of the spreading coefficeint, S [25], [26]. The mass loss term, $\dot{m}$, is given as-

$$\dot{m} = \alpha \left(\frac{M_w}{2\pi RT}\right)^{1/2}\left[p_o \exp\left(\frac{\overline{V}_L}{RT}(-\sigma h_{xx} + \phi)\right) - p_v\right] \tag{2.4}$$

Here in eq.2.1 , the second term corresponds to the mass loss, the first term in the square braces corresponds to the capillary forces and the second term gives the intermolecular interactions. The expression for intermolecular interactions takes into account only Lifshitz-van der Waals forces and acid-base forces. We have also included Born repulsion which we shall see later in this chapter.

2.2.2   Non-dimensionalisation

The evolution equation above contains many physical constants of film liquid such as ρ, μ, S^{LW}, S^P etc. These can be combined together. The non-dimensionalisation is done to study the effect of large number of independent dimensional parameters in terms of less number of independent non-dimensional parameters. The non-dimensionalisation of the evolution equation is done using the following scales-

$$H = \frac{h}{h_o} \qquad d = \frac{d_o}{h_o} \qquad l = \frac{\lambda}{h_o}$$

$$X = \frac{(|A|Ca)^{1/2}x}{h_o} \qquad T = \frac{(A^2Ca)t}{(h_o^2/\nu)}$$

The following nondimensional numbers are also introduced-

$$Ca = \frac{3\rho\nu^2}{\sigma h_o} \qquad A = \frac{-6S^{LW}d^2}{\sigma Ca} \qquad P = -\left(\frac{S^P}{S^{LW}}\right)\left(\frac{1}{6d^2l^2}\right)$$

$\dot{m}$ and ϕ are non-dimensionalised as-

$$M = \frac{1}{p_o}\frac{\dot{m}}{\alpha}\left(\frac{2\pi RT}{M_w}\right)^{\frac{1}{2}}$$

$$\Phi = -\frac{\phi h_o}{6S^{LW}d^2}$$

The evolution equation in its non-dimensional form is obtained as-

$$H_T + C_1 M + \left[H^3 \left(H_{XXX} - sgn\left(A\right) \Phi_H H_X\right)\right]_X = 0 \qquad (2.5)$$

$$M = \exp\left[C_2 \left(-sgn(A)H_{XX} + \Phi\right)\right] - R_1 \qquad (2.6)$$

where, $\qquad \Phi = \dfrac{1}{3}H^{-3} - Pl \exp\left[\dfrac{d-H}{l}\right] \qquad (2.7)$

The non-dimensional parameters obtained are-

$$C_1 = \alpha \left(\frac{M_w}{2\pi RT}\right)^{1/2} \left(\frac{p_o h_o}{\rho v}\right) \left(A^2 Ca\right)^{-1} \qquad (2.8)$$

$$C_2 = \left(\frac{3A\rho v^2}{h_o^2}\right) \left(\frac{\overline{V_L}}{RT}\right) \qquad (2.9)$$

$$R_1 = \frac{p_v}{p_o} \qquad (2.10)$$

The term sgn(A) implies the sign of A. The surface tension term tends to stabilize the film whereas the L-W and acid-base components of the spreading coefficient ($i.e. S^{LW}$ and S^P) describing the intermolecular interactions exert stabilizing or destabilizing effect depending on their sign.

2.2.3 Inclusion of Born Repulsion

There are three types of intermolecular interactions that come into picture for thin films. These are the L-W forces, acid-base forces and the Born repulsion. L-W forces and acid-base forces have already been taken into account. These show a rupture of the film if the energy change at the minimum distance of approach, d_o is negative. But in reality at this distance the Born repulsion always comes into picture which makes the energy change positive below this distance. Here we discuss the criterion for inclusion of Born repulsion, and the changes to be made in the expression for the intermolecular interactions to include the Born repulsion.

- **When to include Born repulsion :**

The expression for ϕ without Born repulsion is given by eq.2.3 as-

$$\phi = \frac{\partial G}{\partial h} = -2S^{LW}\frac{d_o^2}{h^3} - \frac{S^P}{\lambda}\exp\left(\frac{d_o - h}{\lambda}\right)$$

If the energy change is becoming more and more negative as we come to d_o from infinity, it will lead to rupture of the thin liquid film (if Born repulsion is not accounted for). Here ϕ is positive at this point. And, therefore, it becomes the critereon for deciding about the inclusion of Born repulsion.

So we have to include Born repulsion if $\phi(d_o)$ is positive, i.e.,

$$-2S^{LW}\frac{d_o^2}{d_o^3} - \frac{S^P}{\lambda}\exp\left(\frac{d_o - d_o}{\lambda}\right) > 0 \qquad \text{i.e.,}$$

$$-\frac{S^{LW}}{S^P} < \frac{d_o}{2\lambda} \qquad \left(\text{if } S^P \text{ is negative}\right)$$

We also have to include Born repulsion if any of the S^{LW} and S^P is zero and the other is negative (in this situation the ΔG is always negative).

- **How to include Born Repulsion :**

The Born repulsion is included in intermolecular interactions to satisfy the following two constraints at the bare surface (the surface is assumed to be bare when the thickness of the film is 1.37 Å)-

$$\Delta G(l_o) = S^{LW} + S^P \tag{2.11}$$

$$\text{and} \qquad \phi(l_o) = 0 \tag{2.12}$$

This is done by solving the above equation separately for the polar and apolar forces. The energy for intermolecular interactions is written as-

$$\Delta G = \Delta G^{LW} + \Delta G^P$$

For polar forces including Born repulsion,

$$\Delta G^P = c_1 \exp\left(\frac{d_o - h}{\lambda}\right) + \frac{c_2}{h^8} \tag{2.13}$$

6

where c_1 and c_2 are constants to be determined with the following constraints-

$$\Delta G(l_o) = S^P \tag{2.14}$$

$$\text{and} \qquad \phi(l_o) = 0$$

For apolar forces including Born repulsion,

$$\Delta G^{LW} = \frac{c_3}{h^2} + \frac{c_4}{h^8} \tag{2.15}$$

where c_3 and c_4 are constants to be determined with the following constraints-

$$\Delta G(l_o) = S^{LW} \tag{2.16}$$

$$\text{and} \qquad \phi(l_o) = 0$$

The solution of these equations gives the coefficients as-

$$c_1 = S^P \left(1 - \frac{l_o}{8\lambda}\right)^{-1}$$

$$c_2 = -S^P \frac{l_o^9}{8\lambda} \left(1 - \frac{l_o}{8\lambda}\right)^{-1}$$

$$c_3 = \frac{4}{3} S^{LW} l_o^2$$

$$c_4 = -\frac{1}{3} S^{LW} l_o^8$$

These coefficients are further modified by multiplying these by another set of coefficients a_1, a_2, a_3 and a_4 respectively so that we don't incorporate Born repulsion for positive values of S^{LW} or S^P. These coefficients are each equal to 1 if both S^{LW} and S^P are negative. If S^P is positive and S^{LW} is negative, then

$$a_1 = 1 - \frac{l_o}{8\lambda}, \qquad a_2 = 0$$

If S^{LW} is positive and S^P is negative, then

$$a_3 = \frac{3}{4}, \qquad a_4 = 0$$

The equation for ϕ after incorporating Born repulsion and replacing l_o in terms of d_o ($4l_o^2 = 3d_o^2$) is obtained as-

$$\phi = -\frac{a_1}{\lambda} S^P \left(1 - \frac{\sqrt{0.75}d_o}{8\lambda}\right)^{-1} \exp\left(\frac{\sqrt{0.75}d_o - h}{\lambda}\right) +$$

$$\frac{81}{256} \frac{a_2 S^P}{\lambda} \frac{\sqrt{0.75}d_o^9}{h^9} \left(1 - \frac{\sqrt{0.75}d_o}{8\lambda}\right)^{-1} - 2a_3 S^{LW} \frac{d_o^2}{h^3} + \frac{27}{32} a_4 S^{LW} \frac{d_o^8}{h^9} \qquad (2.17)$$

Now we nondimensionalise ϕ by-

$$\Phi = -\frac{\phi h_o}{6 S^{LW} d^2}$$

and the nondimensional form of ϕ is written as-

$$\Phi(H) = Pl \left(1 - \frac{\sqrt{0.75}d}{8l}\right)^{-1} \left[-a_1 \exp\left(\frac{\sqrt{0.75}d - H}{l}\right) + \frac{81\sqrt{0.75}}{256} a_2 \frac{d^9}{H^9}\right]$$

$$+ \left[\frac{1}{3} \frac{a_3}{H^3} - \frac{9}{64} \frac{a_4 d^6}{H^9}\right] \qquad (2.18)$$

where P is non-dimensional number obtained while non-dimensionalising the evolution equation. This is the final expression for nondimensional Φ which we use in eq. 2.5 and eq. 2.6 instead of eq. 2.7. The evolution eaqution is discretised in a set of ordinary differential equations (O.D.E.'s) and then solved. This is discussed next.

- **Discretisation of Evolution Equation**

The initial condition used to solve the evolution equation is-

$$H(X, 0) = 1 + \epsilon \cos(kX)$$

The periodicity interval of the governing eqation 2.5 which is from 0 to $\overline{\lambda}$ is converted to the periodicity interval 0 to 2π by defining a new axial co-ordinate η, such that $\eta = kX$, where k is the wavenumber of the perturbation.

The profile of the interface can be defined by any number of nodes and the evolution eqn. at 'j'th node can be rewritten as-

$$H_T(j) = -C_1 M(j) - k \left[H^3(j) \left(k^3 H_{\eta\eta\eta}(j) - k.sgn(A).\Phi_\eta(j) \right) \right]_\eta$$

The second term on R.H.S. can be rewritten as-

$$k^2 \left[H^3(j) \left(k^2 H_{\eta\eta}(j) - sgn(A).\Phi(j) \right)_\eta \right]_\eta$$

$$= k^2 \left[\frac{F11(j) - F12(j)}{\Delta\eta} \right]$$

where

$$F11(j) = H^3\left(j + \frac{1}{2}\right) \left(k^2 H_{\eta\eta}\left(j + \frac{1}{2}\right) - sgn(A).\Phi\left(j + \frac{1}{2}\right) \right)_\eta$$

$$F12(j) = H^3\left(j - \frac{1}{2}\right) \left(k^2 H_{\eta\eta}\left(j - \frac{1}{2}\right) - sgn(A).\Phi\left(j - \frac{1}{2}\right) \right)_\eta$$

Now these are further discretised as-

$$F11(j) = H^3\left(j + \frac{1}{2}\right) \left[\frac{F21(j+1) - F21(j)}{\Delta\eta} \right]$$

where $\qquad F21(j) = k^2 H_{\eta\eta}(j) - sgn(A)\Phi(j)$

and $\qquad F12(j) = H^3\left(j - \frac{1}{2}\right) \left[\frac{F22(j) - F22(j-1)}{\Delta\eta} \right]$

where $\qquad F22(j) = k^2 H_{\eta\eta}(j) - sgn(A)\Phi(j)$

The second derivative $H_{\eta\eta}$ is calculated as-

$$H_{\eta\eta} = \frac{H(j+1) - 2H(j) + H(j-1)}{(\Delta\eta)^2}$$

The evolution eqution is now fully discretised where everything at any point of time is a function of the height of the film at various points.

2.3 Linear Stability Analysis

The base state is taken as an evaporating (or condensing) flat film [21]. Denoting the base state quantities by an overbar, the equation for base state (from eq. 2.5) is-

$$\overline{H}_{\overline{T}} + C_1 \left[\exp\left(C_2 \overline{\Phi} \right) - R_1 \right] = 0 \tag{2.19}$$

Linearizing eq.2.5 around base state for vanishingly small amplitude of disturbance H' such that-

$$H = \overline{H}(T) + H' \qquad \left(H' << \overline{H} \right)$$

the equation for time evolution of the perturbation H' will be given by [21]-

$$\frac{H'_T}{H'} + \{ \overline{\Phi}_H + sgn(A)k^2 \} \left[C_1 C_2 \overline{\Psi} + sgn(A)k^2 \overline{H}^3 \right] = 0 \tag{2.20}$$

where, $\qquad \overline{\Psi} = \exp\left(C_2 \overline{\Phi} \right)$

For a disturbance of the form-

$$H' = \exp(\omega T + \imath k X)$$

where $\quad \omega =$ growth coefficient, $\quad k =$ non-dimensional wave number, the growth rate (coefficient) will be given by-

$$\omega + \{ \overline{\Phi}_H + sgn(A)k^2 \} \left[C_1 C_2 \overline{\Psi} + sgn(A)k^2 \overline{H}^3 \right] = 0 \tag{2.21}$$

where $\overline{H} = H_o$.

The dominant wave number, k_m, at which surface deformations grow at maximum rate $(\partial \omega / \partial k = 0)$ is given as-

$$k_m^2 = -\frac{C_1 C_2 \overline{\Psi} + \overline{H}^3 \overline{\Phi}_H}{2\ sgn(A)\overline{H}^3} \tag{2.22}$$

Comparing eq.2.22 with dominant wave number derived by Sharma and Jameel[25], it is found that the film considered here for water at 20^0C prefer negligibly larger wavelength deformations largely due to mass loss.

10

2.4 Results and Discussion

• **Numerical Schemes Used :**

The non-dimensional evolution equation which is dicretised in O.D.E.s is solved using the D02EJF routine of the NAG Libraries. This routine solves the O.D.E.s by Gear's method.

2.4.1 Equilibrium Film Thickness

It has been shown earlier [21] that a thin film undergoing evaporation attains a time invariant flat profile due to the balance of attractive (or repulsive) intermolecular forces and mass gain (or loss). The condition for equilibrium film thickness is ($\dot{m} = 0$) which together with eq.2.4 gives-

$$\phi = \frac{RT}{\overline{V}_L} \ln \frac{p_v}{p_o}$$

This equation can be rewritten in the form-

$$2 \left(-\frac{S^{LW}}{S^P} \right) \left(\frac{d_o^2}{h_e^3} \right) - \frac{1}{\lambda} \exp \left[\frac{d_o - h_e}{\lambda} \right] = c$$

$$\text{where} \qquad c = \frac{1}{S^P} \frac{RT}{\overline{V}_L} \ln \frac{p_v}{p_o}$$

It is clear from the above equation that there are multiple roots of this equation as it is non-linear in h_e. Figs. (2) and (5) show these roots for different degrees of saturation. From fig. 2) it is seen that for $c \simeq 0.01$ or less, there are even three roots. If S^{LW} is positive and S^P is negative, then the highest and the lowest of these are stable equilibrium thicknesses and middle one is unstable. This is shown in fig. (3) that a flat film attains a stable equilibrium by evaporation or condensation. The case studied is for the value of c = 0.0001 and $-S^{LW}/S^P = 2.0$. $S^{LW} = 15.0$ dynes/cm and S^P = -7.5 dynes/cm.. If the initial thickness of the film is above the unstable root, it will come to the stable root on the upper side through evaporation or condensation. Also, if the initial thickness is less than the unstable root, it will attain the stable equilibrium on the lower side. If the signs of the values of S^{LW} and S^P are reversed, the behaviour of the roots is also reversed. This is shown in fig. (4) where the both

11

the cases are compared. For negative S^{LW} and positive S^P, the highest and the lowest root are unstable while the middle root is stable. Again from fig. (5) it can be seen that for negative values of 'c' from 0 to -1.0, there are two different roots. The case studied is $-S^{LW}/S^P = 2.0$, $S^{LW} = 15.0$ dynes/cm and S^P = -7.5 dynes/cm, and c = -0.001. For these values, the lower root is stable while the higher root is unstable, fig. (6). If the sign of the values of S^{LW} and S^P is changed for the same value of c, the upper root becomes stable while the lower root becomes unstable, fig. (6). If both the values of S^{LW} and S^P are negative, their is only one root which is unstable, fig. (6).

2.4.2 Instability of Water Films ($S^{LW} > 0, S^P < 0$)

The non-dimensional time evolution equation is solved using the finite difference technique. In the previous work [21] Fourier collocation technique was used to discretise the nonlinear partial differential equation. It was shown that a film of water of mean film thickness of 4 nm at dominating wave number when perturbed slightly undergoes rupture. In the F.C. technique there are some non-physical oscillations at the largely flat portions which cause a spurious rupture. Therefore the finite difference technique has been employed to study these cases. This technique is found to be successful as it clearly shows the "morphological phase separation" of the film ("morphological phase separation" means the formation of a drop in equilibrium with a thin film). This is shown in figs. (7) and (8). The same case is also studied with mass loss. It only hastens the growth of perturbation. The drop is formed alongwith a thin film and due to mass loss the drop decays to a flat film of eq. thickness. This is shown in figs. (9) and (10).

2.4.3 Effect of inclusion of Born Repulsion

Those cases in which the spreading coefficient is negative, the tendency of a perturbed film is to grow in the form of a drop, leaving bare surface on other areas. But at lower thickness, Born repulsion comes into picture (as already discussed when to include Born repulsion). It does not allow the thickness to go below the thickness at the bare surface and thus the evolution of drop and the hole formed can be further studied even after a bare surface is observed.

The cosine wave perturbation of Methylene Iodide film is studied. Here $S^P = 0$ and $S^{LW} = -ve$. Here we have to include the Born repulsion. Figs (11) and (12) show the formation of a drop which further decays to give the bare surface. The maximum angle of the drop with horizontal increases very fast as the drop forms and then it decreases with the decay of the drop. This is shown in Table (1).

The same case is studied at higher degrees of saturation $(p_v/p_o = 0.8)$. Due to higher saturation, mass loss is less. Hence, the drop formed is of larger size and it also takes more time to decay to give the bare surface. This is shown in figs. (13) and (14). Again it is seen that the maximum angle of the drop with horizontal increases very fast as the drop forms and then it decreases with the decay of the drop. This is shown in Table (2).

Fig. 2.1   Physical configuration of a thin film lying on a flat surface

Vapour (2)

h

h_0 $h\,(x\,,\,t)$ **Film (3)**

x

Solid Surface   (1)
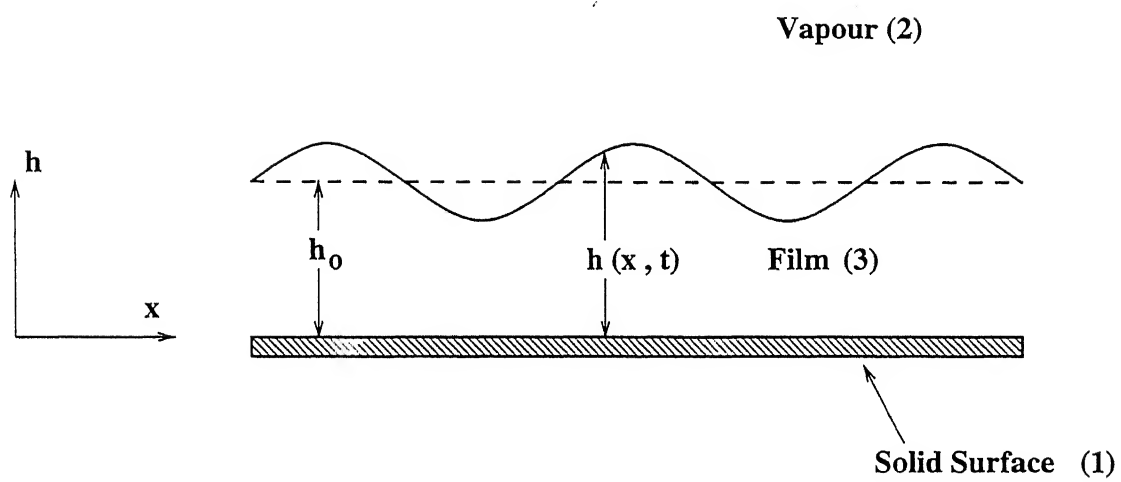
Fig. 2.2 Equilibrium film thicknesses for water at $20^\circ C$ for different degrees of saturation for positive values of 'c'.
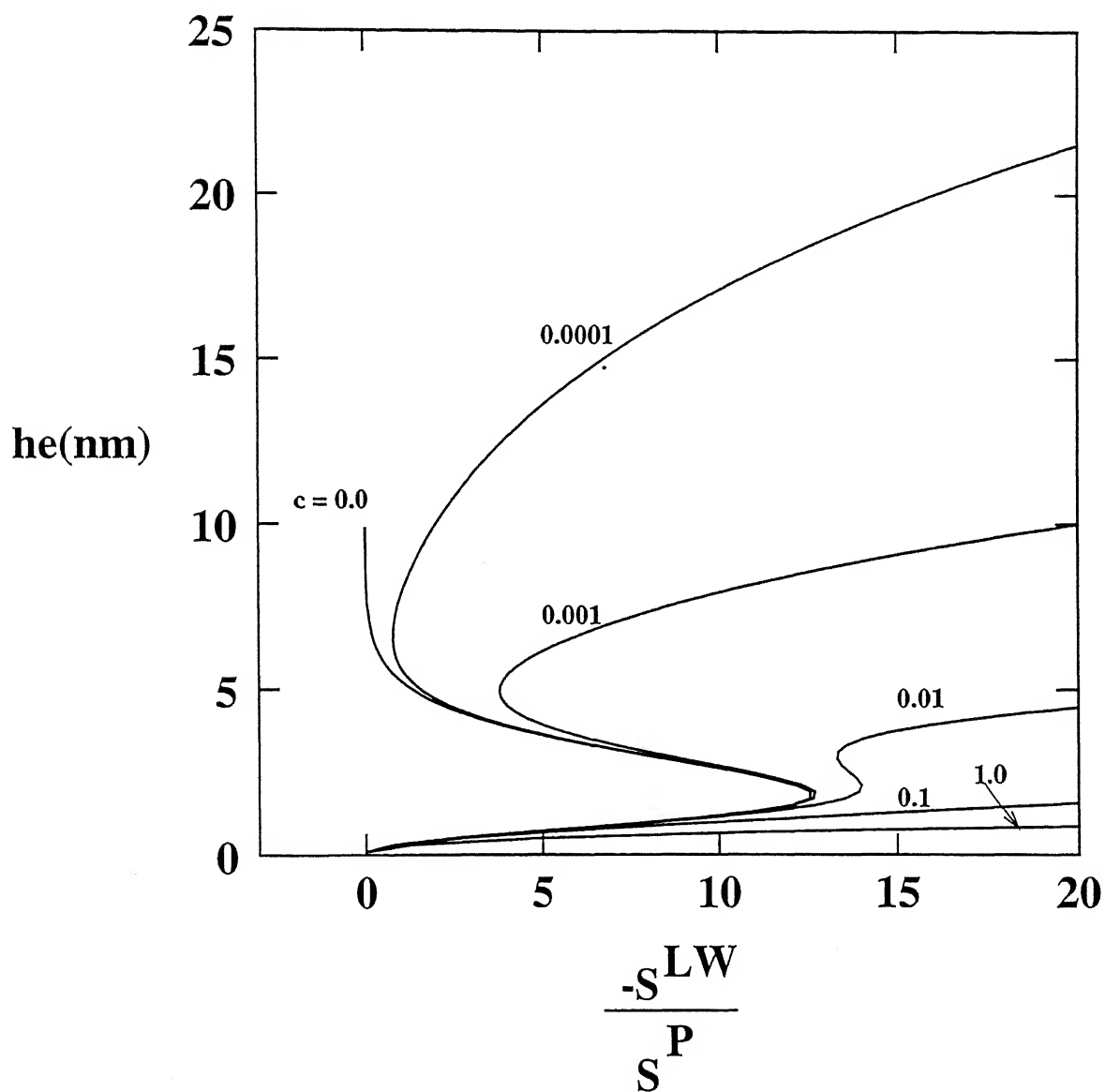
Fig. 2.3 Approach to the stable equilibrium position for a flat film of water. ($S^{LW} = +15.0$ dynes/cm, $S^P = -7.5$ dynes/cm, c = 0.0001)
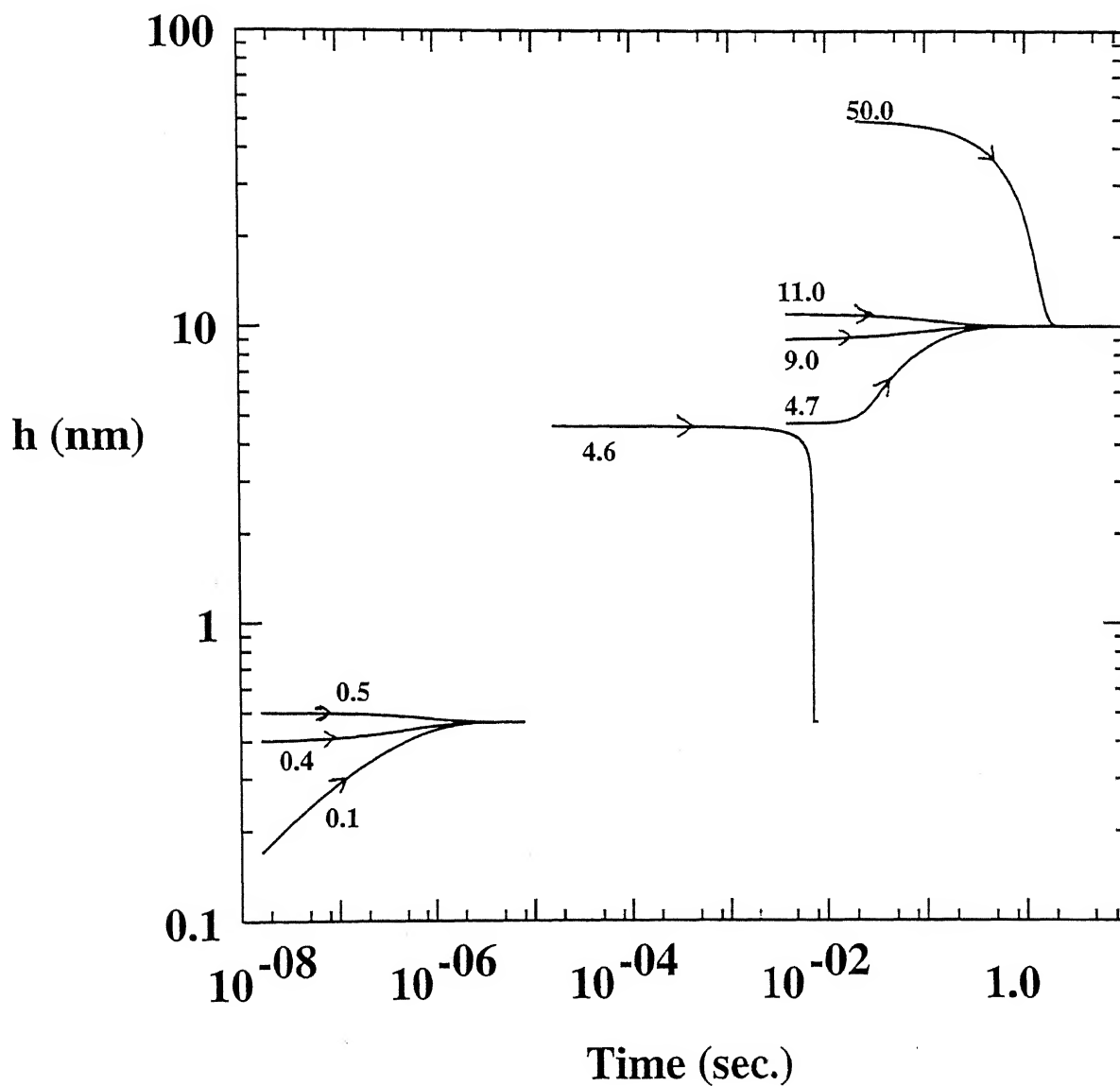
Fig. 2.4 Approach to the stable equilibrium position for a flat film of water-change of stable values of equilibrium thickness. (c = 0.0001)
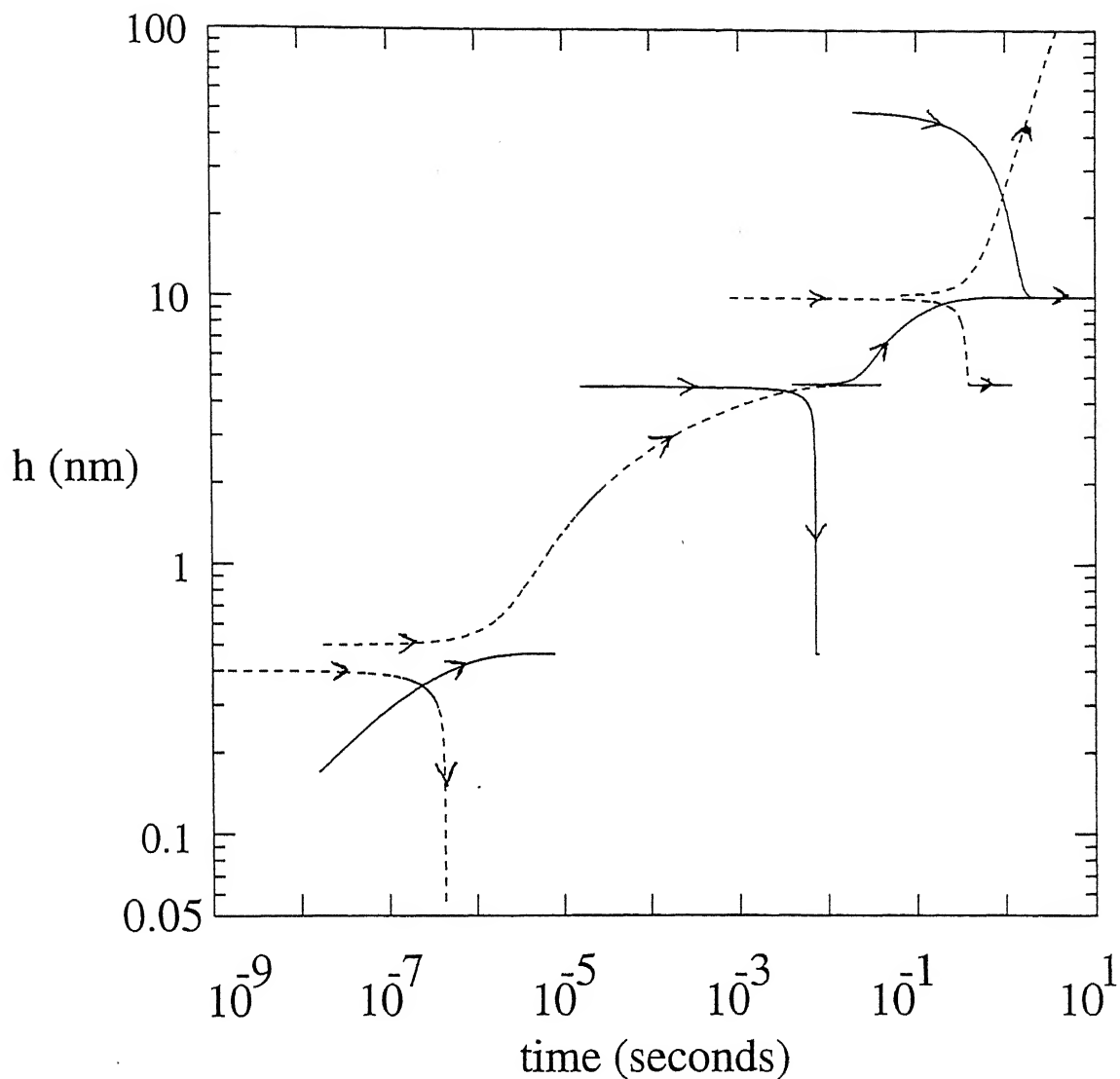
curve	S^{LW}	S^P	p_v / p_o
———	15.0	-7.5	0.99999444
- - - -	-15.0	7.5	1.00000555666

Fig. 2.5   Equilibrium film thicknesses for water at $20^\circ C$ for different degrees of saturation for negative values of 'c'.
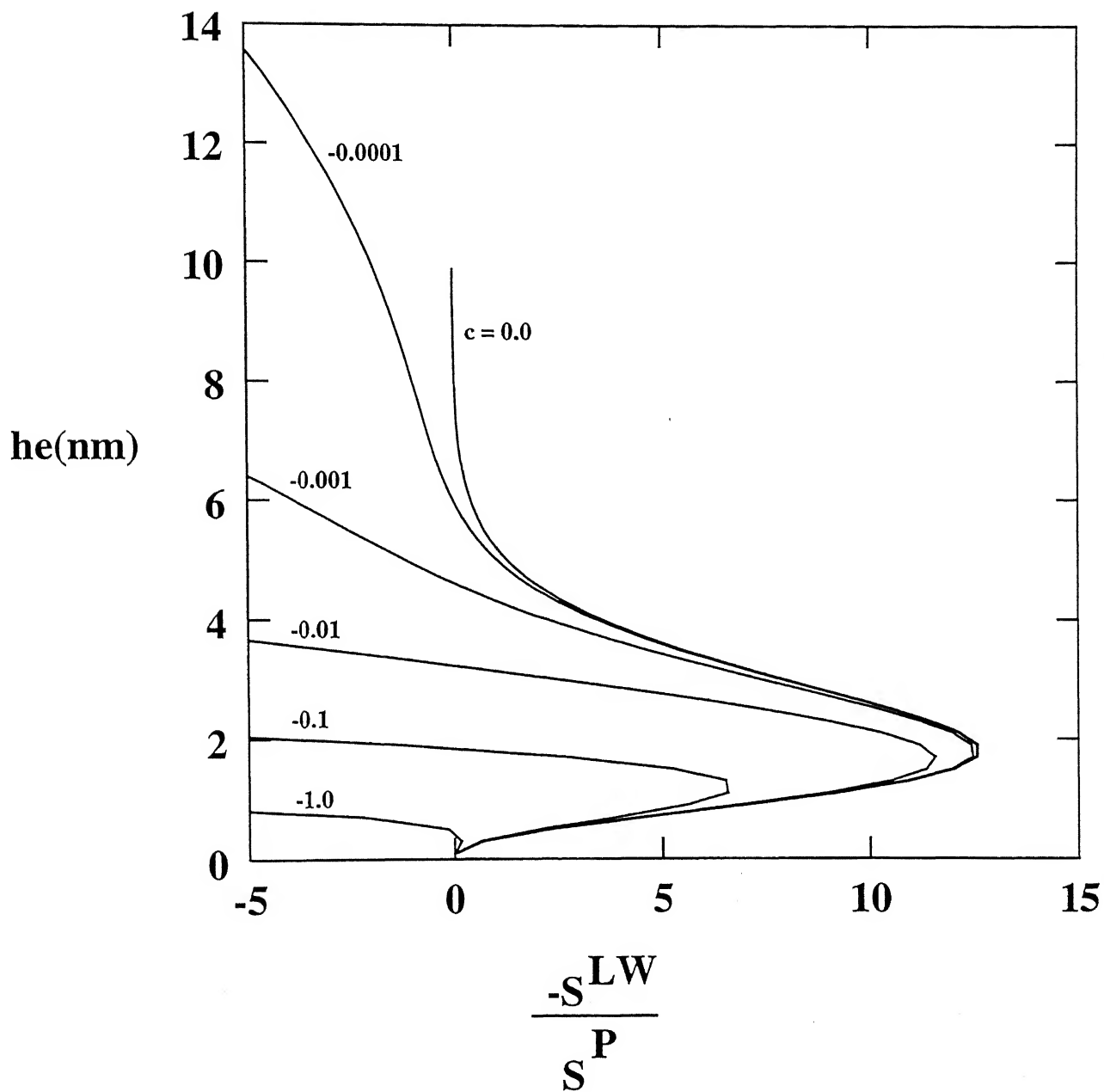
Fig. 2.6 Approach to the stable equilibrium position for a flat film of water-change of stable value of equilibrium thickness. (c = -0.001)
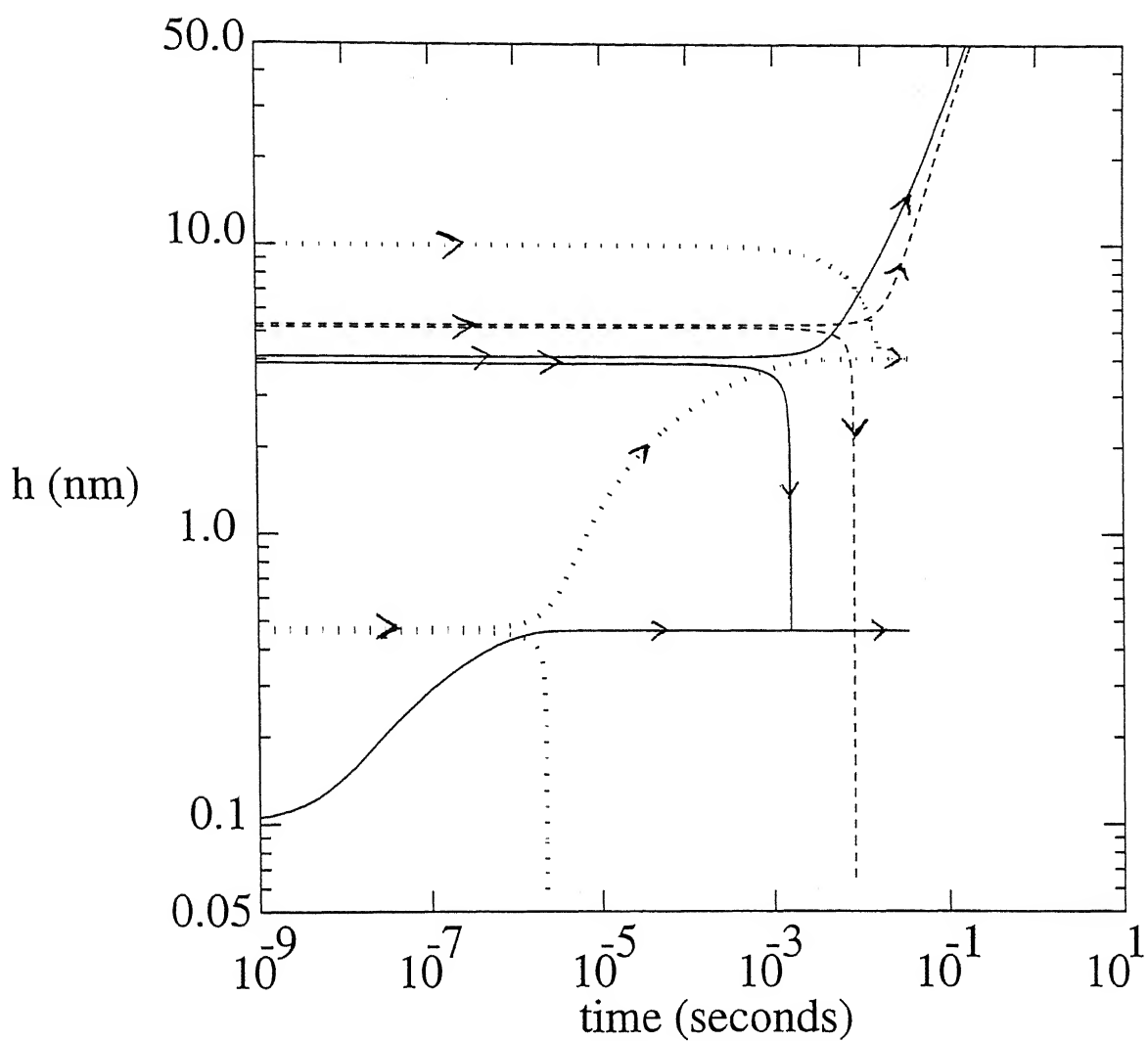
curve	S^{LW}	S^P	p_v / p_o
——	15.0	-7.5	1.00005568
- - - ·	-15.0	-7.5	1.00005568
· · · ·	-15.0	7.5	0.999944435

Fig. 2.7 Film profiles at different intervals of non-dimensional time for a thick film of water neglecting mass loss with $h_o = 4$ nm. ($S^{LW} = +15.46$ dynes/cm, $S^P = $ -30.58 dynes/cm, $p_v/p_o = 0.5$, $C_1 = 53.576$, $C_2 = -2.6807 \times 10^{-4}$, $P = 9.3907 \times 10^3$, $k = k_m = 2.696(30.0519 \mu m^{-1})$)

no.	time
1	0.00
2	0.00598
3	0.01168
4	0.01737
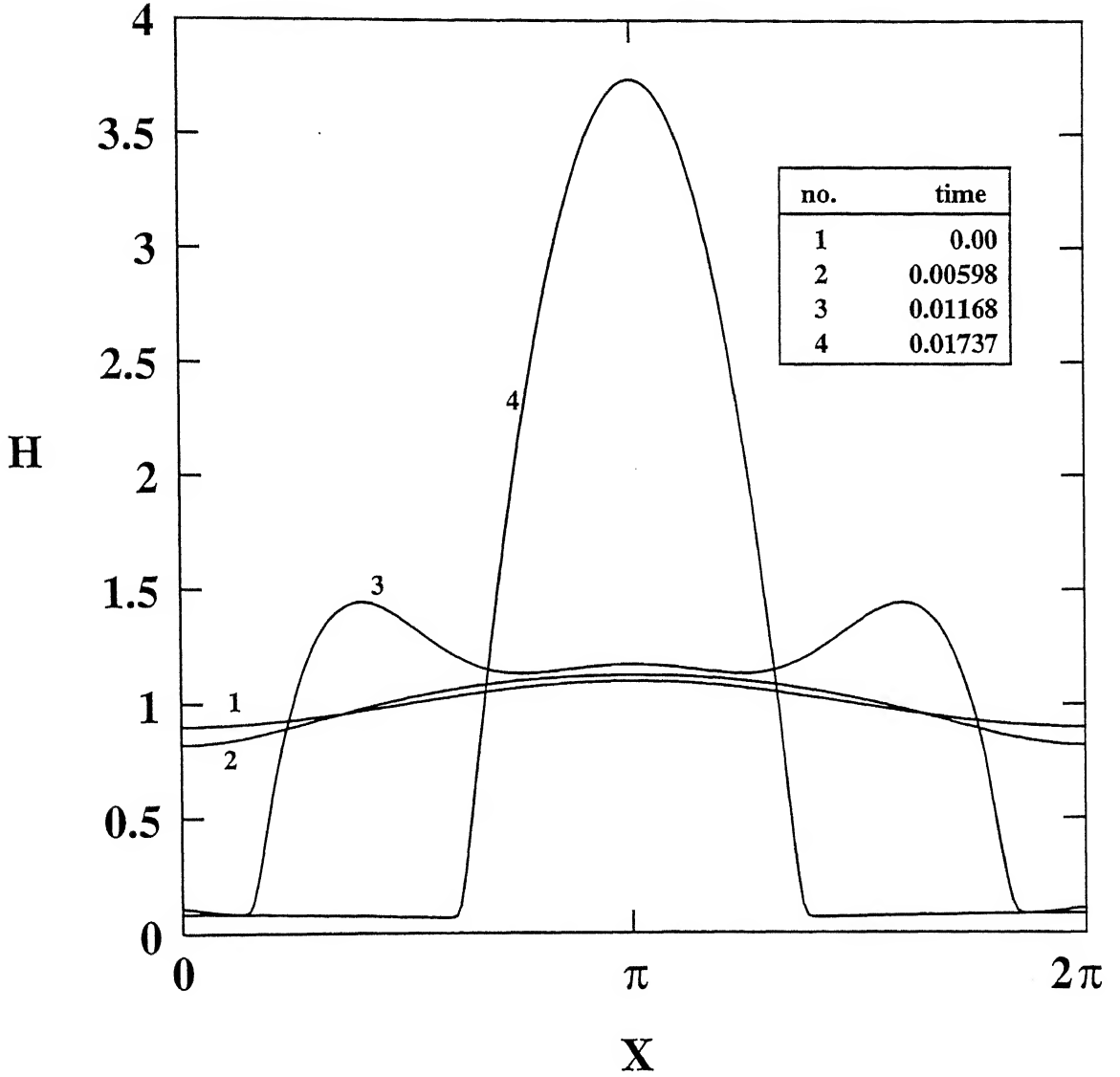
Fig. 2.8 Non-dimensional time evolution for maximum and minimum film thickness for a thick film of water of $h_o = 4$ nm neglecting mass loss. ($S^{LW} = +15.46$ dynes/cm, $S^P = -30.58$ dynes/cm, $p_v/p_o = 0.5$, $C_1 = 53.576$, $C_2 = -2.6807 \times 10^{-4}$, $P = 9.3907 \times 10^3$, $k = k_m = 2.696(30.0519\mu m^{-1})$))
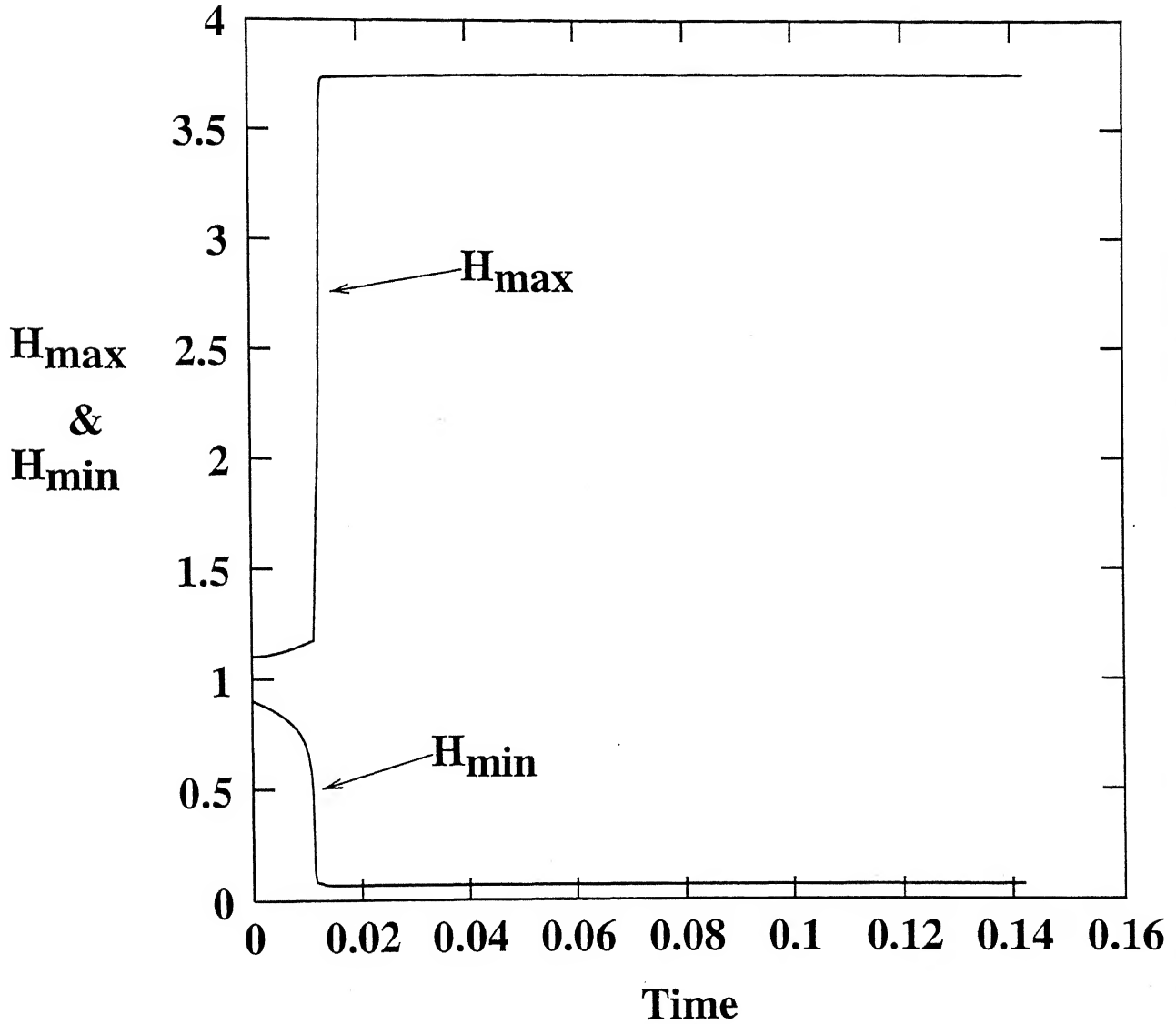
Fig. 2.9 Film profiles at different intervals of non-dimensional time for a thick film of water with $h_o = 4$ nm. ($S^{LW} = +15.46$ dynes/cm, $S^P = -30.58$ dynes/cm, $p_v/p_o = 0.5$, $C_1 = 53.576$, $C_2 = -2.6807 \times 10^{-4}$, $P = 9.3907 \times 10^3$, $k = k_m = 2.696(30.0519 \mu m^{-1})$))

no.	time
1	0.00000
2	0.00598
3	0.01168
4	0.03988
5	0.06836
6	0.08557
7	0.10266
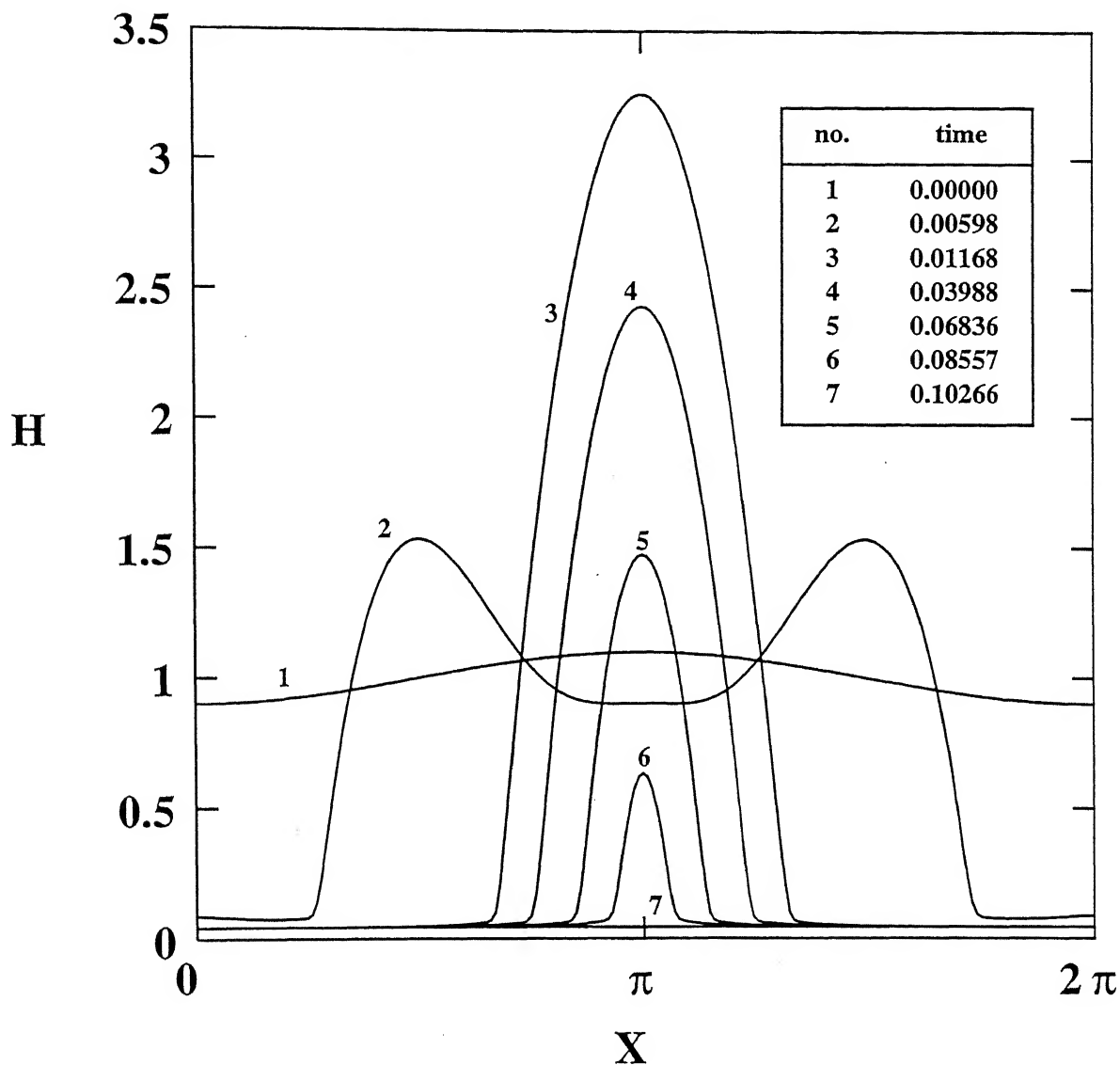
Fig. 2.10 Non-dimensional time evolution for maximum and minimum film thickness for a thick film of water of $h_o = 4$ nm. ($S^{LW} = +15.46$ dynes/cm, $S^P = $ -30.58 dynes/cm, $p_v/p_o = 0.5$, $C_1 = 53.576$, $C_2 = -2.6807 \times 10^{-4}$, $P = 9.3907 \times 10^3$, $k = k_m = 2.696(30.0519 \mu m^{-1})$)
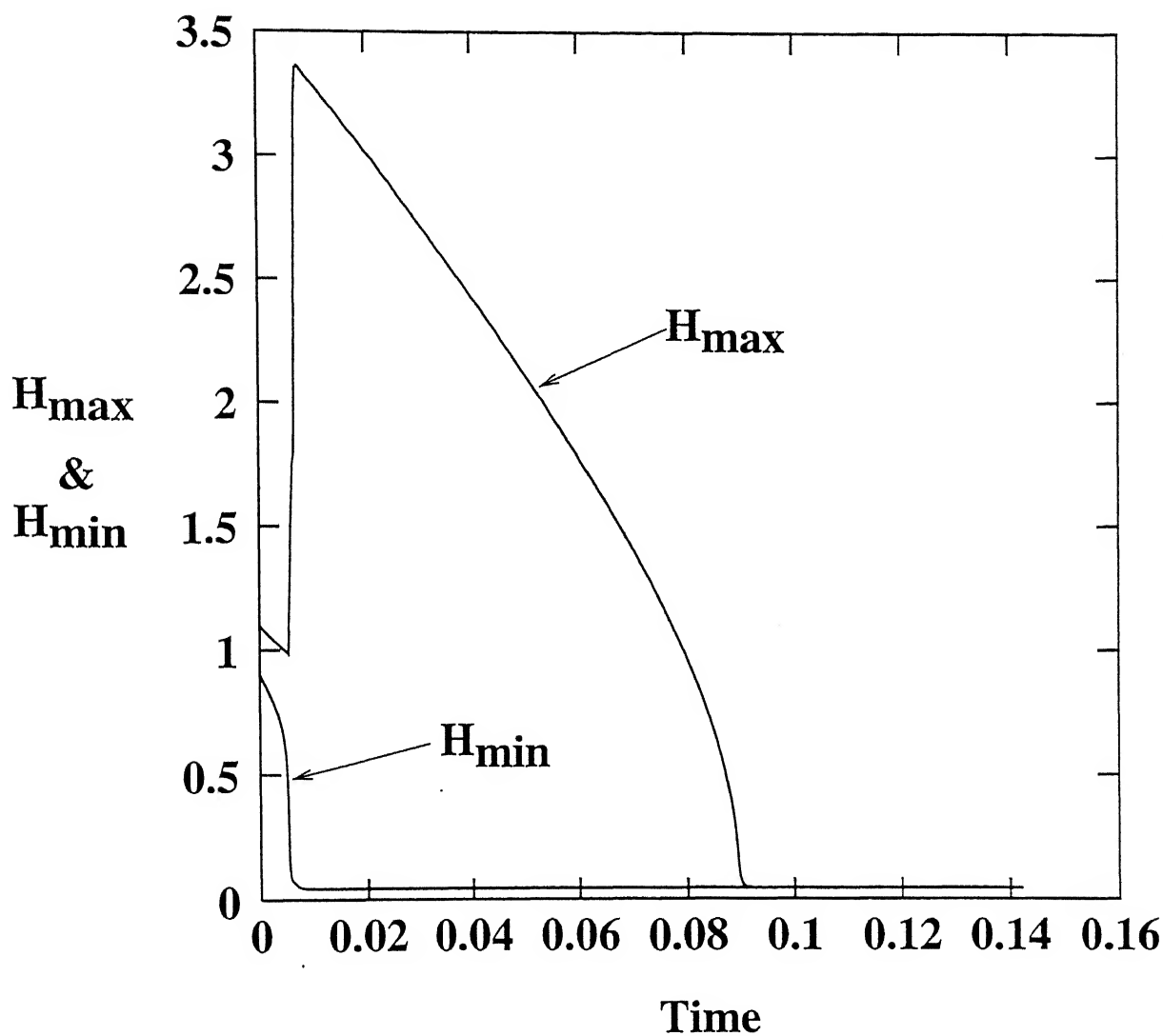
Fig. 2.11 Film profiles at different intervals of non-dimensional time for a thin film of methylene iodide with $h_o = 2$ nm. ($S^{LW} = $ -20.0 dynes/cm, $S^P = 0$ dynes/cm, $p_v/p_o = 0.5$, $C_1 = 0.2945$, $C_2 = 1.2384 \times 10^{-2}$, P = 0, $k = k_m = 0.7058(42.8466 \mu m^{-1})$)

no.	time
1	0.00
2	1.68
3	1.76
4	1.92
5	8.00
6	12.20
7	16.20
8	20.20
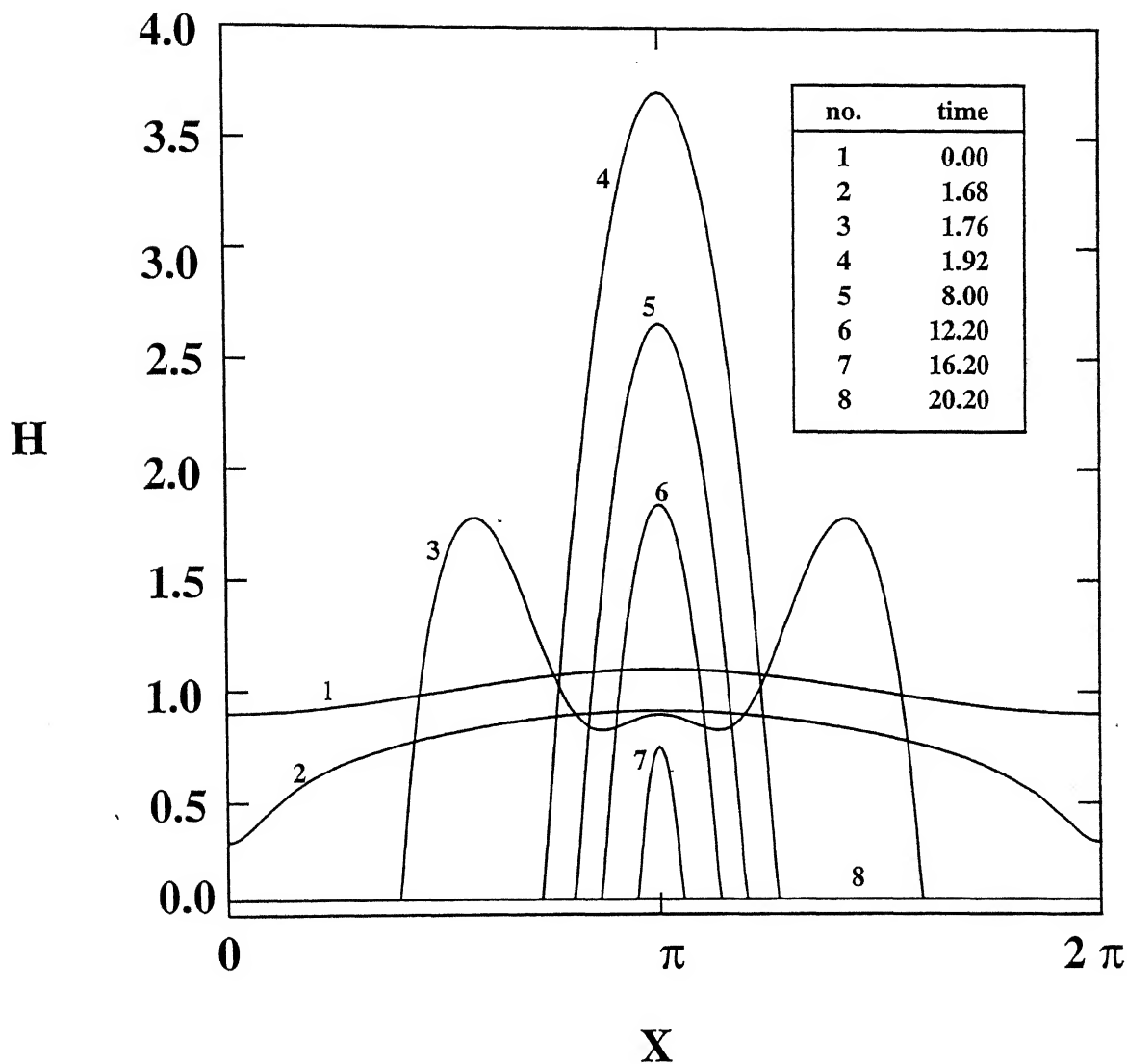
Fig. 2.12 Non-dimensional time evolution for maximum and minimum film thickness for a thin film of methylene iodide of $h_o = 2$ nm. ($S^{LW} = -20.0$ dynes/cm, $S^P = 0$ dynes/cm, $p_v/p_o = 0.5$, $C_1 = 0.2945$, $C_2 = 1.2384 \times 10^{-2}$, P = 0, $k = k_m = 0.7058(42.8466 \mu m^{-1})$))
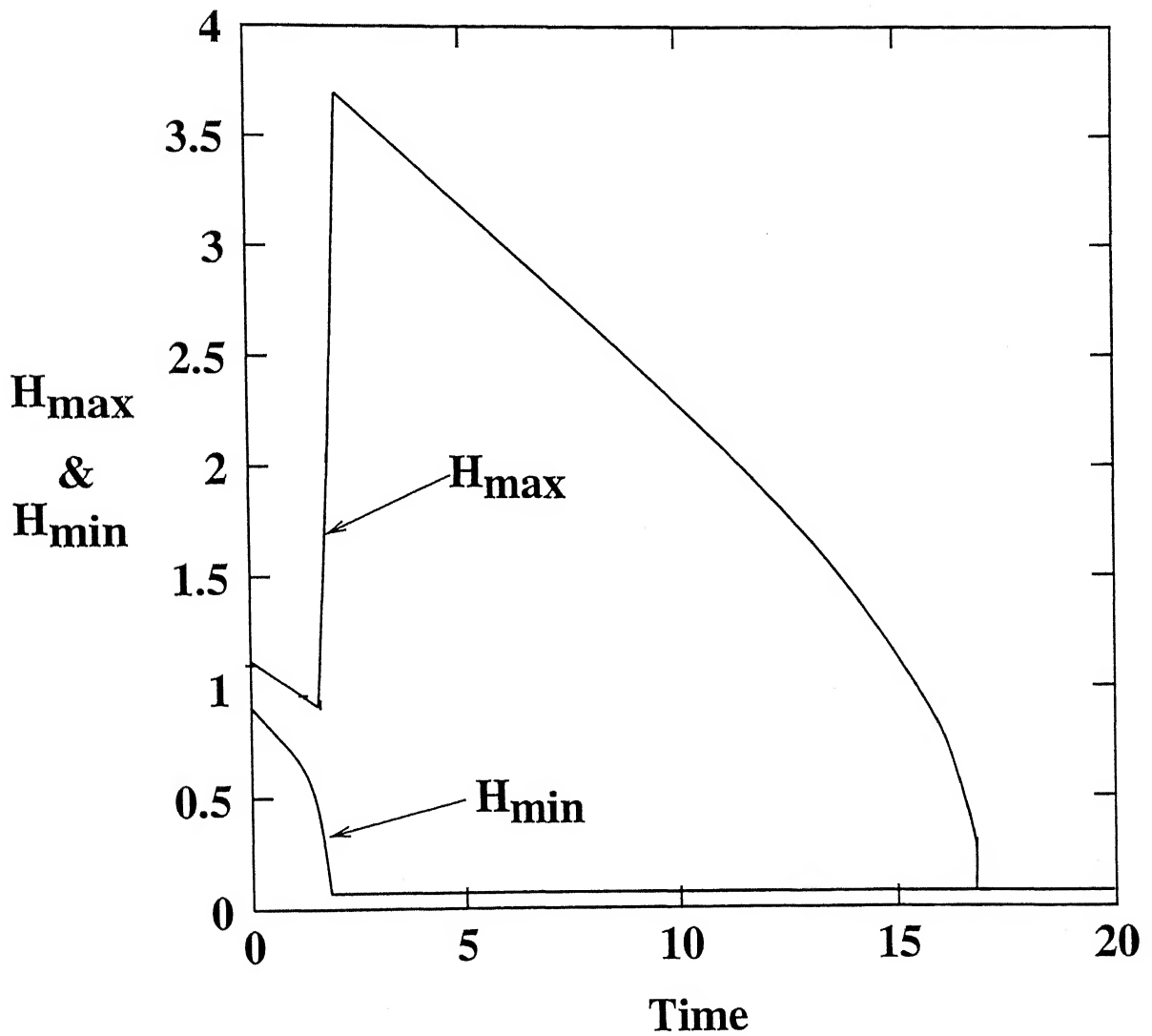
Fig. 2.13 Film profiles at different intervals of non-dimensional time for a thin film of methylene iodide with $h_o = 2$ nm. ($S^{LW} = $ -20.0 dynes/cm, $S^P = 0$ dynes/cm, $p_v/p_o = 0.8$, $C_1 = 0.2945$, $C_2 = 1.2384 \times 10^{-2}$, P = 0, $k = k_m = 0.7058(42.8466 \mu m^{-1})$))

no.	time
1	0.00
2	2.41
3	2.61
4	13.20
5	25.20
6	33.20
7	37.20
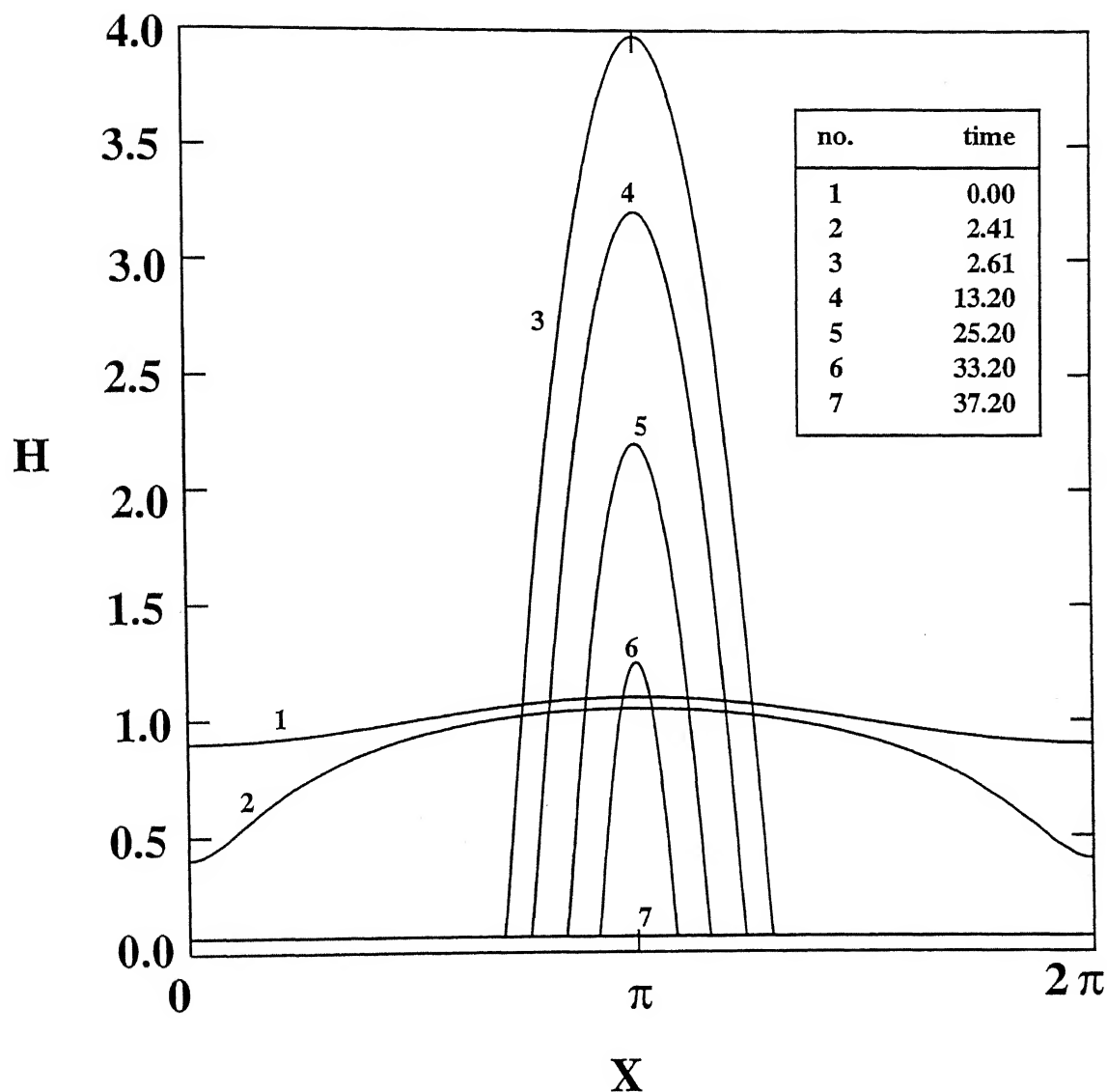
Fig. 2.14 Non-dimensional time evolution for maximum and minimum film thickness for a thin film of methylene iodide of $h_o = 2$ nm. ($S^{LW} = -20.0$ dynes/cm, $S^P = 0$ dynes/cm, $p_v/p_o = 0.8$, $C_1 = 0.2945$, $C_2 = 1.2384 \times 10^{-2}$, P = 0, $k = k_m = 0.7058(42.8466 \mu m^{-1})$))
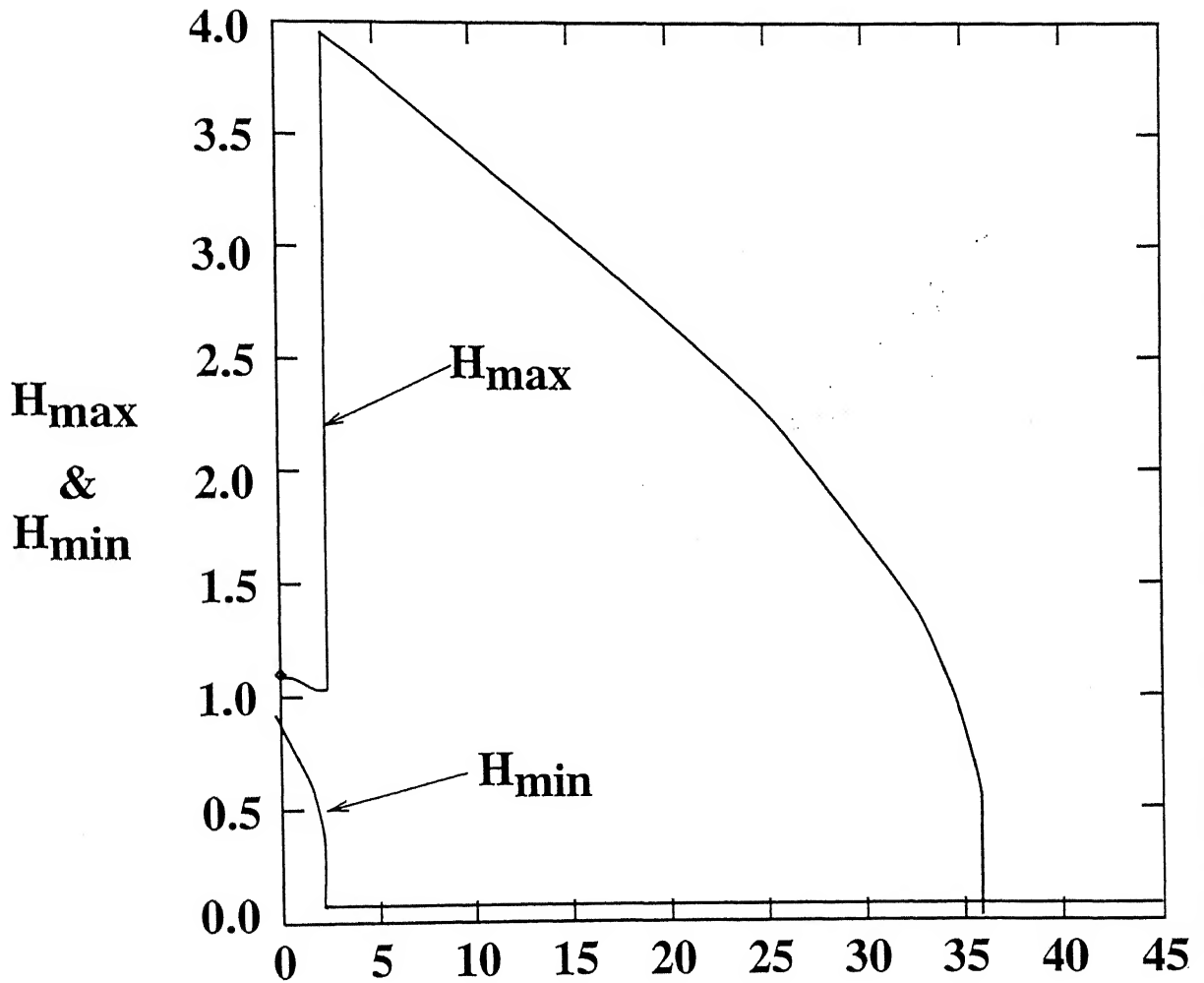
Table 2.1: Evolution of a film of Methylene Iodide ($h_o = 2$ nm, $S^{LW} = -20$ dynes/cm, $S^P = 0$, $p_v/p_o = 0.5$)

Time (non-dim.)	H_{max} (non-dim.)	H_{min} (non-dim.)	θ_{max} (degrees)	Volume (nm^3/nm)
0.00	1.1000	0.90000	0.6956	206.9927
0.40	1.0491	0.82330	0.7844	194.6849
1.68	0.9133	0.32460	4.1546	155.0271
1.76	1.7811	0.06784	41.1801	152.5958
1.84	3.6574	0.06784	42.6166	151.1661
1.92	3.7069	0.06784	43.6565	150.2107
4.00	3.3167	0.06784	42.4440	126.2408
8.00	2.6574	0.06784	42.3941	84.5866
12.00	1.8406	0.06784	41.2241	47.5116
16.00	0.7501	0.06784	37.6601	18.9100
20.00	0.06784	0.06784	0.0000	14.0407

Table 2.2: Evolution of a film of Methylene Iodide ($h_o = 2$ nm, $S^{LW} = $ -20 dynes/cm, $S^P = 0$, $p_v/p_o = 0.8$)

Time (non-dim.)	H_{max} (non-dim.)	H_{min} (non-dim.)	θ_{max} (degrees)	Volume (nm^3/nm)
0.00	1.1000	0.90000	0.6956	206.9927
1.60	1.0557	0.70548	1.2704	186.9852
2.40	1.0516	0.40356	3.5844	176.7264
2.60	3.9741	0.06822	43.1171	174.4047
4.40	3.8901	0.06822	43.7611	164.1590
4.80	3.8360	0.06822	43.3039	161.9120
13.00	3.2071	0.06822	42.9510	117.0160
33.00	1.2503	0.06822	41.8087	28.0880
37.00	0.06822	0.06822	0.0000	14.1200

Chapter 3

Heterogeneous Nucleation : Circular Critical Nucleii

3.1 Introduction

This chapter essentially deals with the situation where the critical nucleus is assumed to be a circular drop lying on a flat film. The study is made by considering the initial profile of a drop lying on a flat film and then see whether it grows or decays. By this study we are able to find a critical nucleus which will grow under the conditions prevailing .

3.2 Generation of Initial Profile

The initial profile is taken as a part of a circular drop lying on a flat film of thickness 1.37 Å(fig. 1). The equilibrium contact angle θ is found from the relation :

$$\cos(\theta) = 1 + \frac{S}{\gamma}$$

where S is the spreading coefficient $\left(S = S^{LW} + S^P\right)$ [25], [26].

Different initial profiles are generated for different heights of the drop (h_o) above the film.

3.3 Formulation Of Problem

The time evulution eqn. describing the behaviour of the drop is the same as shown in previous chapter. The only difference is that there is no need to consider the wave number as we are dealing with a different initial profile now. The non-dimensionalisation is done w.r.t. the top thickness of the drop above the liquid film, h_o. The evolution eqn. is :

$$H_T + C_1 M + \left[H^3 \left(H_{XXX} - sgn\left(A\right) \Phi_H H_X \right) \right]_X = 0 \qquad (3.1)$$

and

$$M = \exp\left[C_2 \left(-sgn\left(A\right) H_{XX} + \Phi \right) \right] - R_1 \qquad (3.2)$$

The initial profile is defined as in the fig. (1). The growth and decay of different nucleii with varying size are studied. The results are discussed in the next section .

3.4 Results and Discussion

To find a critical nucleus we study the growth/decay of a drop. The top thickness of a drop (h_o) is varied. This gives different nucleii of varying radius of curvature. A typical case study is shown for the parameters : $S^{LW} = 15$ dynes/cm, $S^P = -30$ dynes/cm, $p_v/p_o = 1.0224$. The study shows that the nucleii with radius of curvature greater than 315 Åwill grow and those with radius of curvature less than 292 Åwill decay. This is shown in fig. (2) and (3). It is observed that the drop initially grows both in vertical and lateral dimensions. When it grows sufficiently in the lateral dimension, it starts interacting with the neighbouring drops and grows as a flat film. If we consider the drop to be lying in a larger pool of flat film as shown in fig.(4), the growth of the drop in vertical as well as lateral dimensions is more before it starts interacting with the neighbouring drops and grow as a flat film. This is evident from

comparing fig.(2) and fig.(4).

The study is also made for two more cases with $S^P = $ - 40 dynes/cm and -70 dynes/cm while other parameters remaining the same. In the former case the critical nucleus is found to have a radius of curvature between 276 Å and 285 Å, while in the latter case the critical nucleus is found to have a radius of curvature between 262 Å and 284 Å. The equilibrium contact angle increases with S^P becoming more -ve , which means a larger critical nucleus. This is as predicted by the simulation results and shown in fig. (5).

Fig. 3.1 Physical configuration of a drop lying on a thin film on a solid substrate.
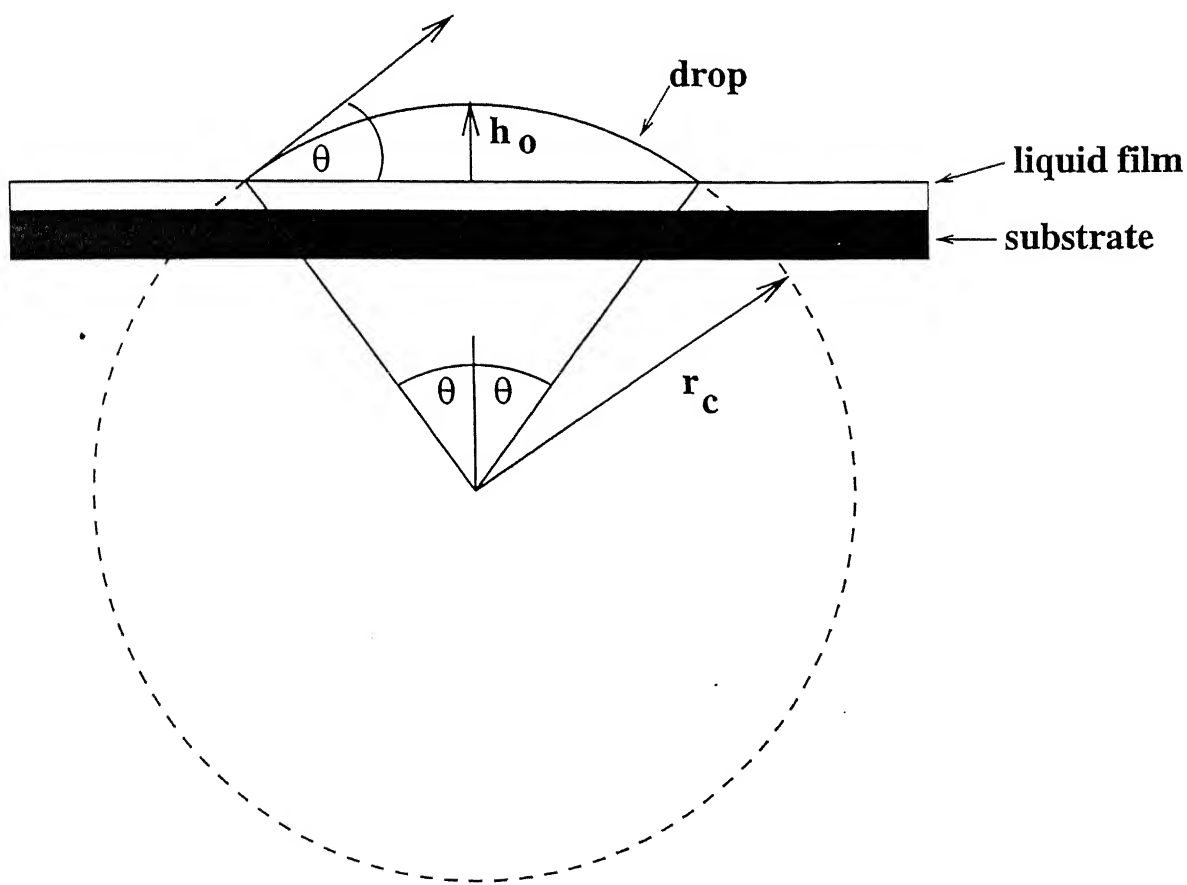
Fig. 3.2   Growth of a drop with radius of curvature $= 315$ A. ($S^{LW} = +15$ dynes/cm, $S^P = -30$ dynes/cm, $p_v/p_o = 1.0224$.)
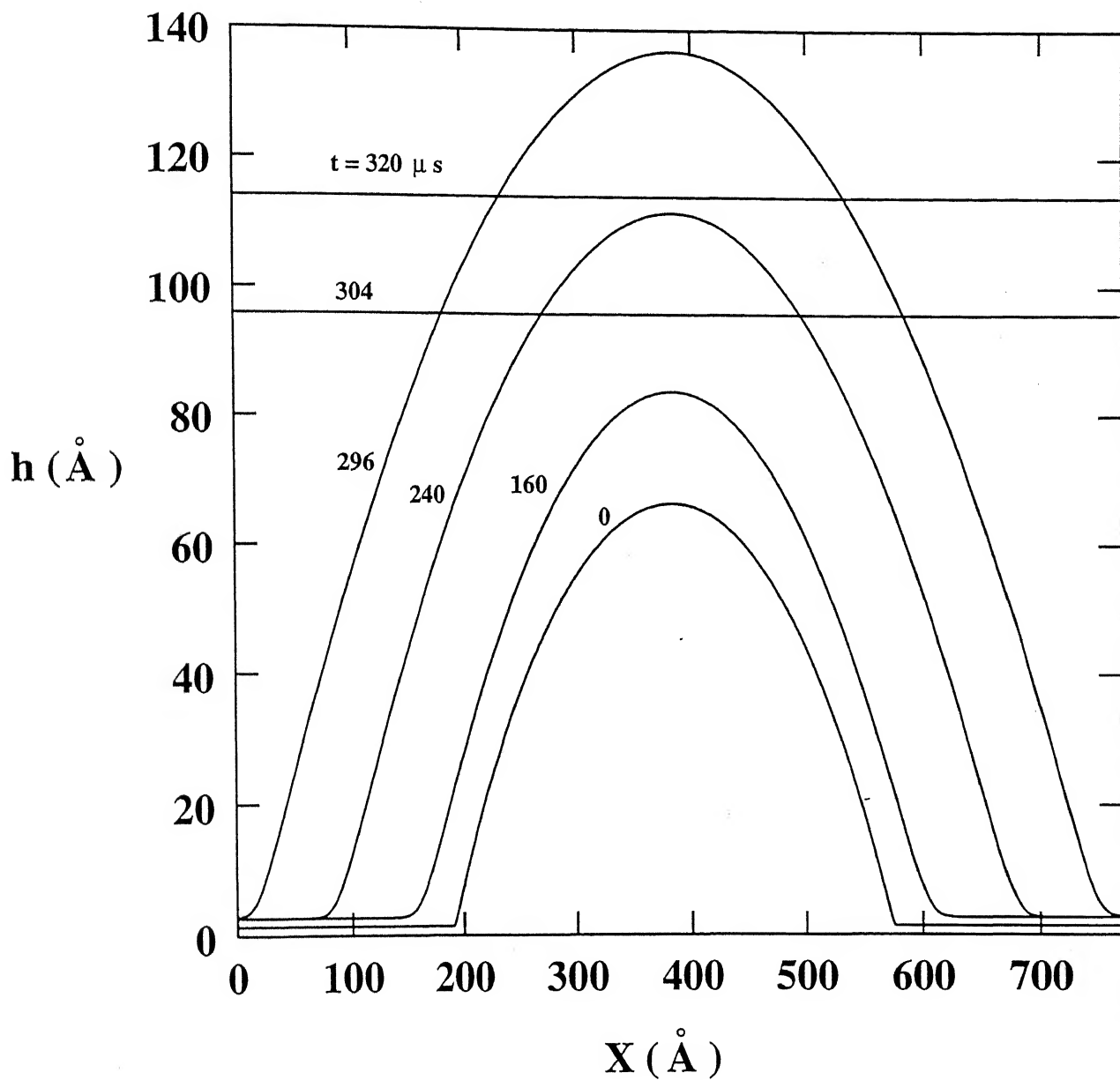
Fig. 3.3 Decay of a drop with radius of curvature = 292 A. ($S^{LW} = +15$ dynes/cm, $S^P = $ -30 dynes/cm, $p_v/p_o = 1.0224$.)

no.	t (μs)
1	0.0
2	36.0
3	54.0
4	57.6
5	61.2
6	64.8
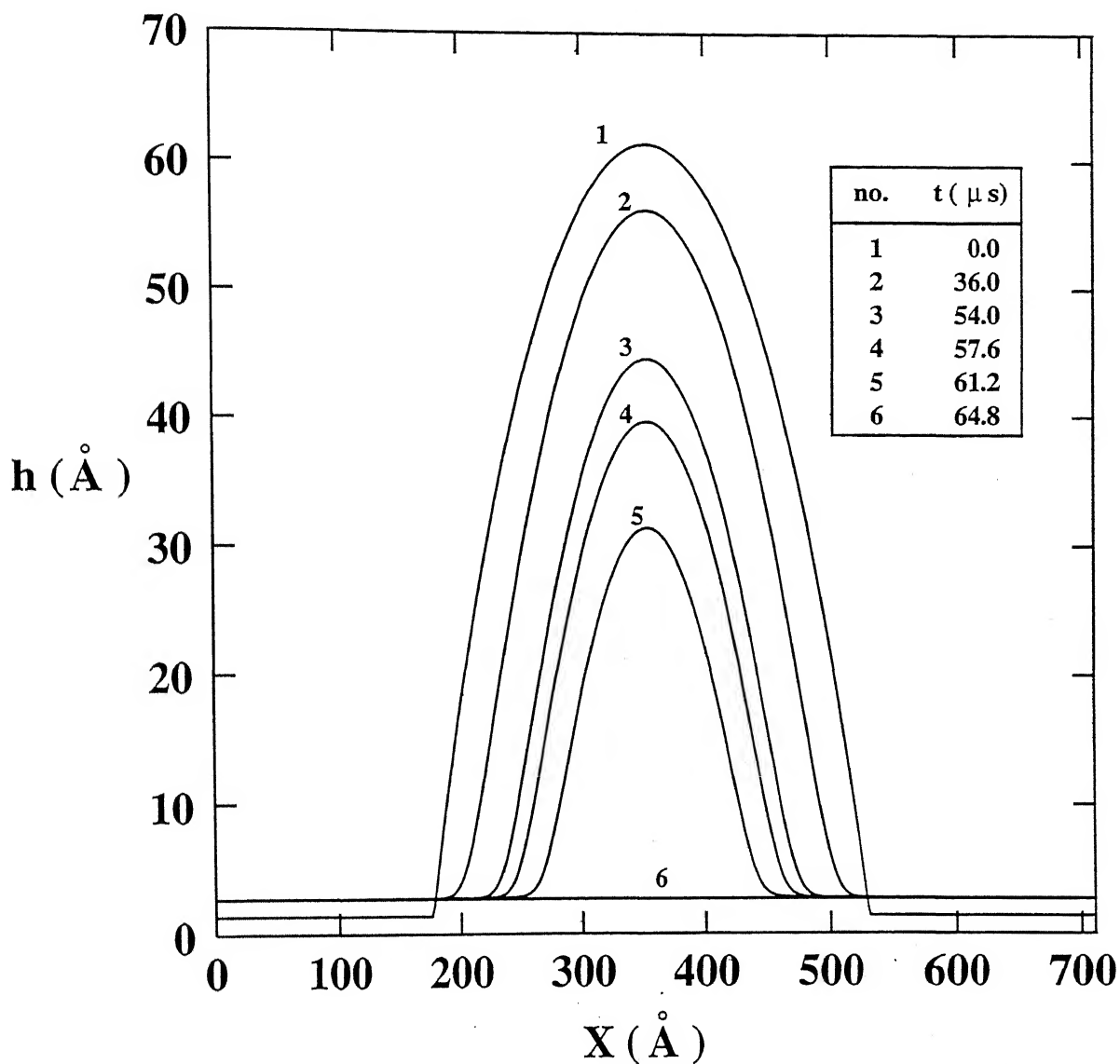
Fig. 3.4 Growth of a drop in a larger pool of flat film with radius of curvature $= 315$ A. ($S^{LW} = +15$ dynes/cm, $S^P = -30$ dynes/cm, $p_v/p_o = 1.0224$.)
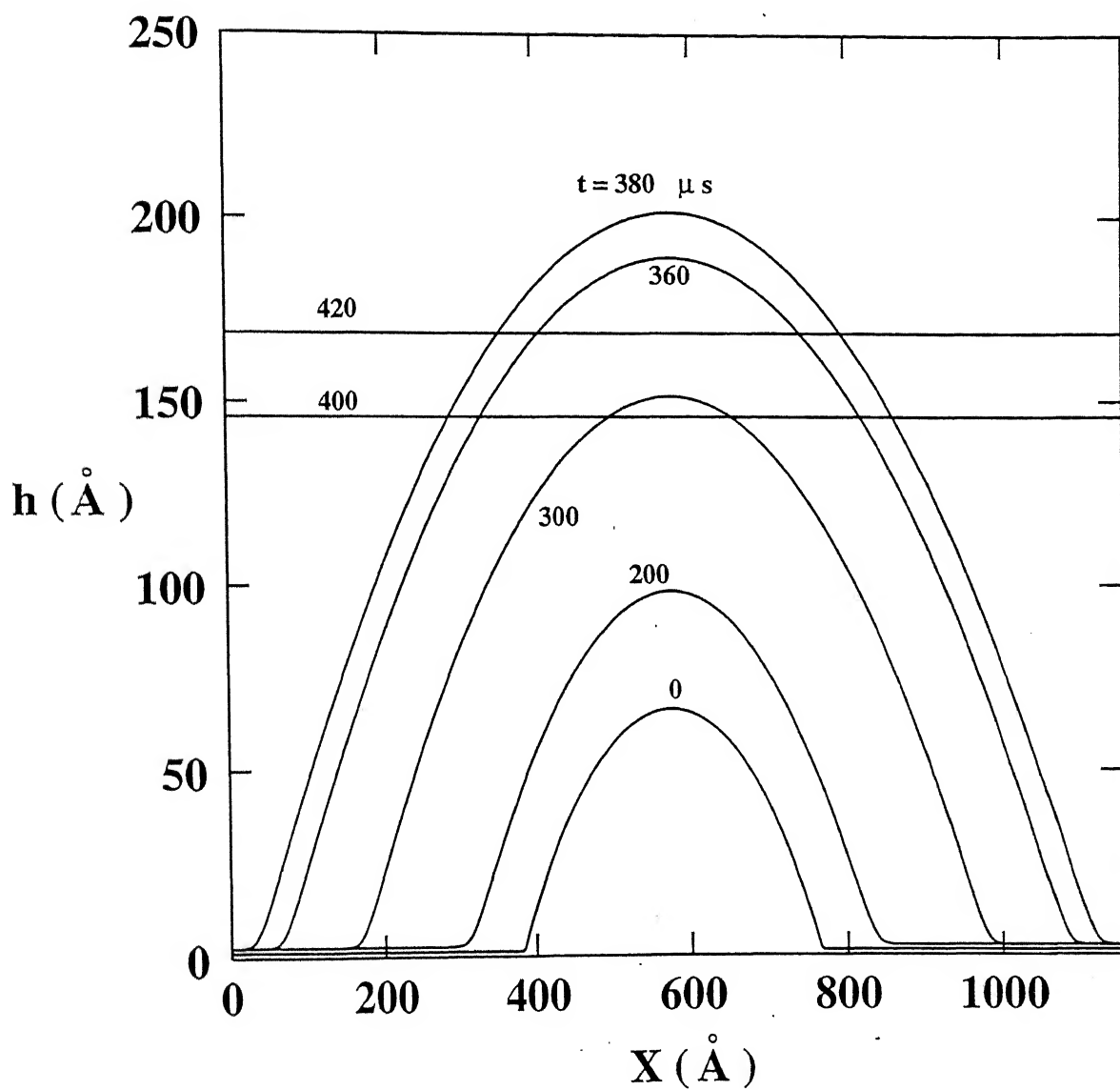
Fig. 3.5 Critical nucleii for different values of S^P. ($S^{LW} = +15$ dynes/cm, p_v/p_o = 1.0224.)

no.	S^P (dynes/cm)
1	-30
2	-40
3	-70
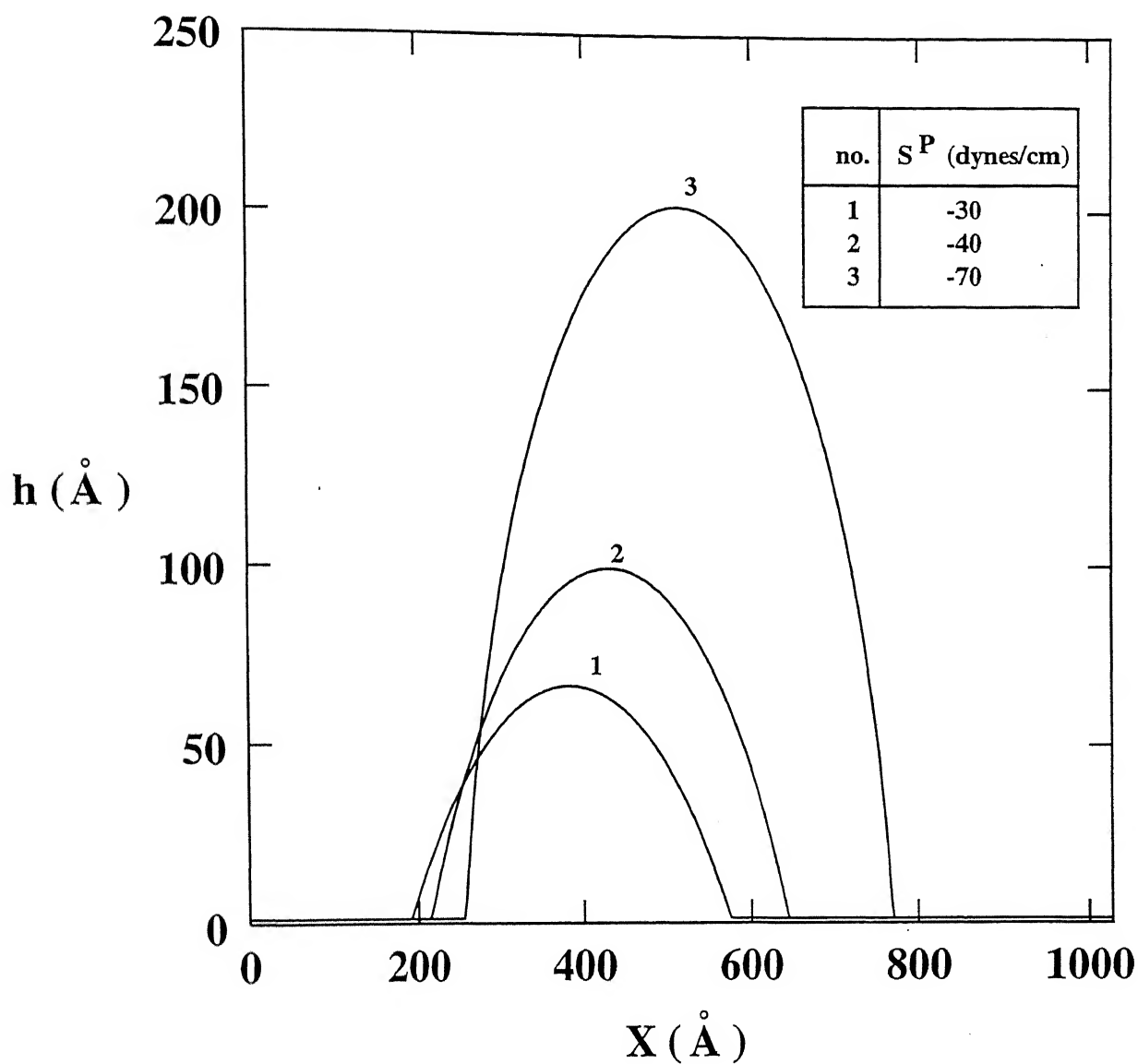
Chapter 4

Heterogeneous Nucleation : Energy Considerations

4.1   Introduction

In the previous chapter we have seen how to obtain a critical nucleus which is of the shape of a circular drop. But so far no consideration has been given to the energy associated with it. The critical nucleus need not be necessarily of a circular shape. It may have any shape. Critical nucleii of different shapes have different amounts of energy associated with them. It is, therefore, of great importance to find a critical nucleus which requires minimum amount of energy for its generation. This chapter deals with the generation of a critical nucleus with minimum energy, observing the growth or decay of drops near the critical nucleus and study the effects of various parameters on the size of the critical nucleus.

4.2   Formulation of the Problem

4.2.1   Generation of the Critical Profile with Minimum Energy

When the mass loss or mass gain at every point of a profile is zero, it means that it is an equilibrium profile. This may be a stable or unstable equilibrium. An unstable equilibrium is one which when slightly perturbed, either grows or decays depending

on the perturbation. The mass-loss term at any point is given by:

$$\dot{m} = \alpha \left(\frac{M_w}{2\pi RT}\right)^{1/2} \left[p_o \exp\left[\frac{\overline{V}_L}{RT}\left(\frac{-\sigma h_{xx}}{(1+h_x^2)^{3/2}} + \phi\right)\right] - p_v\right] \qquad (4.1)$$

At equilibrium, $\dot{m} = 0$, which gives:

$$h_{xx}\left(1 + h_x^2\right)^{-3/2} + \frac{RT}{\overline{V}_L\gamma}\ln\frac{p_v}{p_o} - \frac{\phi}{\gamma} = 0 \qquad (4.2)$$

As a flat film of thickness h_e is also a solution of this equation, and $h_{xx} = 0$ at h_e, so we get-

$$\frac{\phi(h_e)}{\gamma} = \frac{RT}{\overline{V}_L\gamma}\ln\frac{p_v}{p_o} = K_o \qquad \text{(a constant)} \qquad (4.3)$$

The solution of this equation gives the eq. thickness, h_e.

The equation4.2 when integrated, gives us

$$\left(1 + h_x^2\right)^{-1/2} + \frac{\Delta G}{\gamma} - K_o h + c = 0 \qquad (4.4)$$

$$\text{or} \qquad h_x = [(K_o h - \frac{\Delta G(h)}{\gamma} - c)^{-2} - 1]^{1/2} \qquad (4.5)$$

This equation is used to generate the critical profile, details of which will be discussed while explaining the results. Now, to obtain c, h_o and R_o, we proceed as follows:

At $x = x_c$ (where the drop is at its maximum height, fig. 1), we have $h = h_o$ and $h_x = 0$. Therefore, from equation4.4

$$1 + \frac{\Delta G(h_o)}{\gamma} - K_o h_o + c = 0 \qquad (4.6)$$

At $x = -\infty$, we have $h = h_e$ and $h_x = 0$. Therefore, from equation4.4

$$1 + \frac{\Delta G(h_e)}{\gamma} - K_o h_e + c = 0 \qquad (4.7)$$

From these two equations, we get:

$$\Delta G(h_e) + \gamma K_o(h_o - h_e) = \Delta G(h_o) \tag{4.8}$$

The solution of this equation gives the top thickness of the drop, i.e., h_o. Also we get the constant c from any of the two equations above.

At $x = 0$, we have $h = h_o,$ $\qquad h_x = 0$ and $\qquad h_{xx} = \frac{-1}{R_o}$

therefore, from equation4.2, we get:

$$\frac{-1}{R_o} - \frac{\phi(h_o)}{\gamma} + K_o = 0$$

$$\text{or} \qquad R_o = (K_o - \frac{\phi(h_o)}{\gamma})^{-1} \tag{4.9}$$

So we get the radius of curvature of the critical nucleus at the top.

4.2.2 Calculation of Energy Required to Generate the Critical Nucleus

The energy required to create a nucleus is given by the difference of the energy associated with a nucleus lying on a thin film (fig. 1) and that with a flat film only.

For a flat film:

$$F_i = (\gamma_L + \gamma_{SL})A + \Delta G(h_e)A - Ah_e\frac{RT}{\overline{V}_L}\ln\frac{p_v}{p_o} \tag{4.10}$$

For the drop lying on a flat film:

$$F_c = 2\gamma_l \int_0^{x_c}(\sqrt{1+h_x^2})dx + A\gamma_{SL} + 2\int_0^{x_c}\Delta G(h)dx - 2\frac{RT}{\overline{V}_L}\ln\frac{p_v}{p_o}\int_0^{x_c}hdx \tag{4.11}$$

The energy required to generate the nucleus is then:

$$\Delta F = F_c - F_i$$

or

$$\Delta F = \left[2 \int_0^{x_c} \Delta G(h) dx - \Delta G(h_e) A \right] + \left[2\gamma_l \int_0^{x_c} (\sqrt{1 + h_x^2}) dx - 2\gamma_L x_c \right]$$

$$- \frac{2RT}{\overline{V}_L} \ln \frac{p_v}{p_o} \left[\int_0^{x_c} h dx - h_e x_c \right]$$

or

$$\Delta F = \left[2 \int_0^{x_c} (\Delta G(h) - \Delta G(h_e)) dx \right] + \left[2\gamma_l \int_0^{x_c} (\sqrt{1 + h_x^2} - 1) dx \right]$$

$$- \frac{2RT}{\overline{V}_L} \ln \frac{p_v}{p_o} \left[\int_0^{x_c} (h - h_e) dx \right] \qquad (4.12)$$

where the integral $\int_0^{x_c} (\sqrt{1 + h_x^2} dx$ gives the area of half the drop.

This is the energy required to generate a profile over a flat film, the profile being defined from x = 0 to x = x_c. This equation is used to give the energy required to generate critical nucleii, both from continuumm approach and the classical approach.

Continuum Approach

The critical nucleus which requires minimum energy for its generation is given by the solution of equation4.5 in the range x = 0 to x_c using 'd02ejf ' subroutine from theNAG librararies (to be discussed in the results section). Equation4.12 is then used to get the energy required as:

$$\Delta F_{crit} = \left[2 \int_0^{x_c} \Delta G(h) dx - \Delta G(h_e) A \right] + \left[2\gamma_l \int_0^{x_c} (\sqrt{1 + h_x^2}) dx - 2\gamma_L x_c \right]$$

$$- \frac{2RT}{\overline{V}_L} \ln \frac{p_v}{p_o} \left[\int_0^{x_c} h dx - h_e x_c \right] \qquad (4.13)$$

41

Classical Approach

In the classical theory, the drop is assumed to be large enough so that we can consider the $\Delta G(h)$ to be negligible (which is not true for smaller drops as we will see in the results). The drop is assumed to be a circular one (fig. 2). x_c is replaced by R_1, r_c is the radius of curvature of the circular drop, θ is the equilibrium contact angle and $\Delta G(h_e)$ is replaced by $\gamma_l(\cos\theta - 1)$. So from equation4.12 we get the energy required to generate a critical profile of circular shape as:

$$\Delta F = -\frac{1}{2}r^2\left[2\theta - \sin 2\theta\right]\frac{RT}{\overline{V}_L}\ln\frac{p_v}{p_o} + 2r\sin\theta\left[\frac{\gamma_l\theta}{\sin\theta} - \gamma_l\cos\theta\right]$$

For ΔF to be minimum, $\frac{\partial \Delta F}{\partial r} = 0$, which gives radius of curvature as:

$$r_c = \frac{2\gamma_l\sin\theta\left(\frac{\theta}{\sin\theta} - \cos\theta\right)}{(2\theta - \sin 2\theta)\frac{RT}{\overline{V}_L}\ln\frac{p_v}{p_o}} \tag{4.14}$$

and the corresponding energy required is:

$$\Delta F^* = -\frac{1}{2}r_c^2\left[2\theta - \sin 2\theta\right]\frac{RT}{\overline{V}_L}\ln\frac{p_v}{p_o} + 2r_c\sin\theta\left[\frac{\gamma_l\theta}{\sin\theta} - \gamma_l\cos\theta\right] \tag{4.15}$$

The energy required for a critical nucleus as from continuum approach and classical approach are then compared which is discussed next in section Results and Discussion.

4.3   Results and Discussion

- **Numerical Schemes Used to Solve Different Equations.**

Different subroutines from the NAG Libraries have been used to solve different equations. In addition to the D02EJF routine for solving stiff O.D.E.s, two more routines are used - D01GAF and C05ADF.

- **D01GAF**

This routine integrates a function which is specified numerically at 4 or more points, over the whole range specified. It uses third order finite difference formulae according to a method due to Gill and Miller.

- C05ADF

This routine locates a zero of a function in a given interval by a combination of the methods of linear interpolation, extrapolation and bi-section.

- **Effect of Equilibrium Contact Angle :**

The increase in the equilibrium contact angle, θ, means that the wettability of the surface is decreasing. This reduces the effect of surface on the heterogeneous nucleation and, therefore, we need a larger critical nucleus which can grow. As the size of the critical nucleus increases, it supports our assumption in classical theory that $\Delta G(h)$ can be neglected. So the energy required as predicted by the classical theory(ΔF^*) comes closer to the that predicted by the continuum approach. ΔF_{crit} (shown by simulation results).

We have studied the effect of changing different parameters on the energy required to generate the critical nucleus both from the classical theory and from the continuum approach. The study is made for three different situations:

1. Liquid - Water , $S^P = 0$, S^{LW} = -ve ;
2. Liquid - Octane , $S^P = 0$, S^{LW} = -ve ;
3. Liquid - Water , S^P = -ve , S^{LW} = +ve ;

The study of all these situations supports the concept that any change that leads to an increase in θ results in larger critical nucleus and also less discrepancy between the energy required to generate the critical nucleus from both the theories.

- **1. Liquid - Water , $S^P = 0$, S^{LW} = -ve**

When $S^P = 0$ and S^{LW} is negative, then the spreading coefficient is negative and we have to include Born Repulsion. As it is evident from the relation $\cos(\theta) = 1 + \frac{\Delta G(h_e)}{\gamma}$, and $\Delta G(h_e) = S^{LW} + S^P$ in this case, that as S^{LW} becomes more and more negative, the contact angle θ increases which results in larger and larger critical nucleus. This concept is clear from fig. (3) in which we have shown the critical nucleus for different values of S^{LW}.

Next we study the effect of increasing p_v/p_o (higher saturation). At higher saturation a smaller critical nucleus is required which could grow. This is again supported by the results as shown in fig. (4) and (5). Different cases have been studied for p_v/p_o ranging from 1.1 to 2.0.

The discrepancy in the energy required to generate a critical nucleus as predicted from classical theory and from continuumm approach decreases at higher θ and vice-versa. The discrepancy is measured in terms of the ratio of the ΔF_{crit} and ΔF^*. We have seen that as p_v/p_o increases, the size of the critical nucleus decreases which does not support the assumption of classical theory that $\Delta G(h)$ can be considered negligible. Therefore, the discrepancy increases with increase in relative saturation. Also, when S^{LW} is made more and more negative, the contact angle increases which implies a larger critical nucleus size and, hence, less discrepancy. These concepts are supported by the results shown in fig. (6) .

Next we show how a slight perturbation in the critical nucleus affects its growth or decay. The behaviour of the nucleus is studied in the same way as in previous chapter except that the non-dimensionalisation is done w.r.t. the top thickness of the drop above the flat solid surface. Fig. (7) shows the growth of a nucleus the height of which is 5% more than the critical nucleus at every point. Initially the drop grows and then it becomes a flat film (due to interactions with neighbouring drops). Then it grows as a flat film. Fig. (8) shows the decay of a nucleus the height of which is 1% less than the critical nucleus at every point. The drop continuously decays and

becomes a flat film of equilibrium thickness, h_e.

The results of someof the parameter variations are shown in table 1.

- **2. Liquid - Octane , $S^P = 0$, $S^{LW} = $ -ve**

Another case is studied where the liquid is Octane. Here also we have to include Born repulsion. The variation in contact angle is studied and shown directly in fig (9). It is showing clearly that the discrepancy decreases as contact angle increases. Also at the same contact angle, if surface tension is increased , S^{LW} becomes more -ve correspondingly (to keep θ same) . This results in the reduction in wettability of surface. Therefore the critical nucleus size increases and discrepancy decreases. Two different sets of curves are drawn for $p_v/p_o = 2$ and $p_v/p_o = 3$. The discrepancy increases with increase in p_v/p_o for the same reasons as cited before . Fig. (10) shows the discrepancy over a wider range of p_v/p_o. The increase in the size of critical nucleus with S^{LW} becoming more and more negative is shown in fig.(11). Figs. (12) and (13) show the growth and decay of a critical nucleus if it is slightly perturbed. The growth is observed for 5% higher perturbation at every point and decay is observed for 1% lower perturbation at every point.

The results of some of the parameter variations are shown in table 2.

- **3. Liquid - Water , $S^P = $ -ve , $S^{LW} = $ +ve**

When the effect of different parameters is studied in case of water taking polar forces into account, we don't have to include Born repulsion in the parameters range studied. Fig.(14) and (15) show the decrease in discrepancy with increase in the equilibrium contact angle. Also, the discrepancy increases with increase in relative saturation. Fig.(16) shows the same thing for a higher range of p_v/p_o. Fig (17) and (18) show the growth and decay of a critical nucleus if it is slightly perturbed. The growth is observed for 5% higher perturbation at every point and decay is observed

for 1% lower perturbation at every point. Results of some of the parameter variations are shown in table 3.

Fig. 4.1   Physical configuration of nucleus of liquid on flat solid surface.
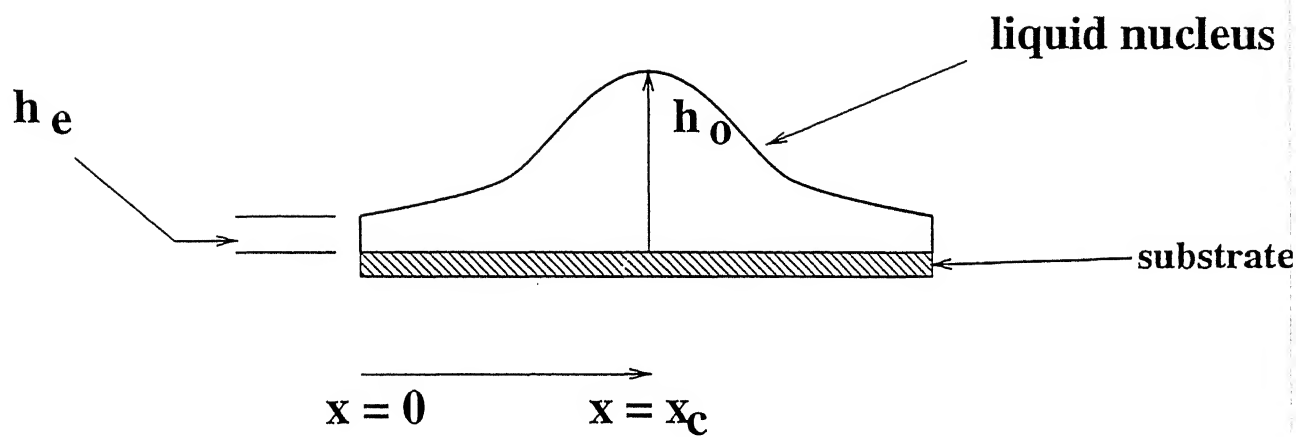
Fig. 4.2   Physical configuration of a circular drop lying on thin film on a solid
surface.
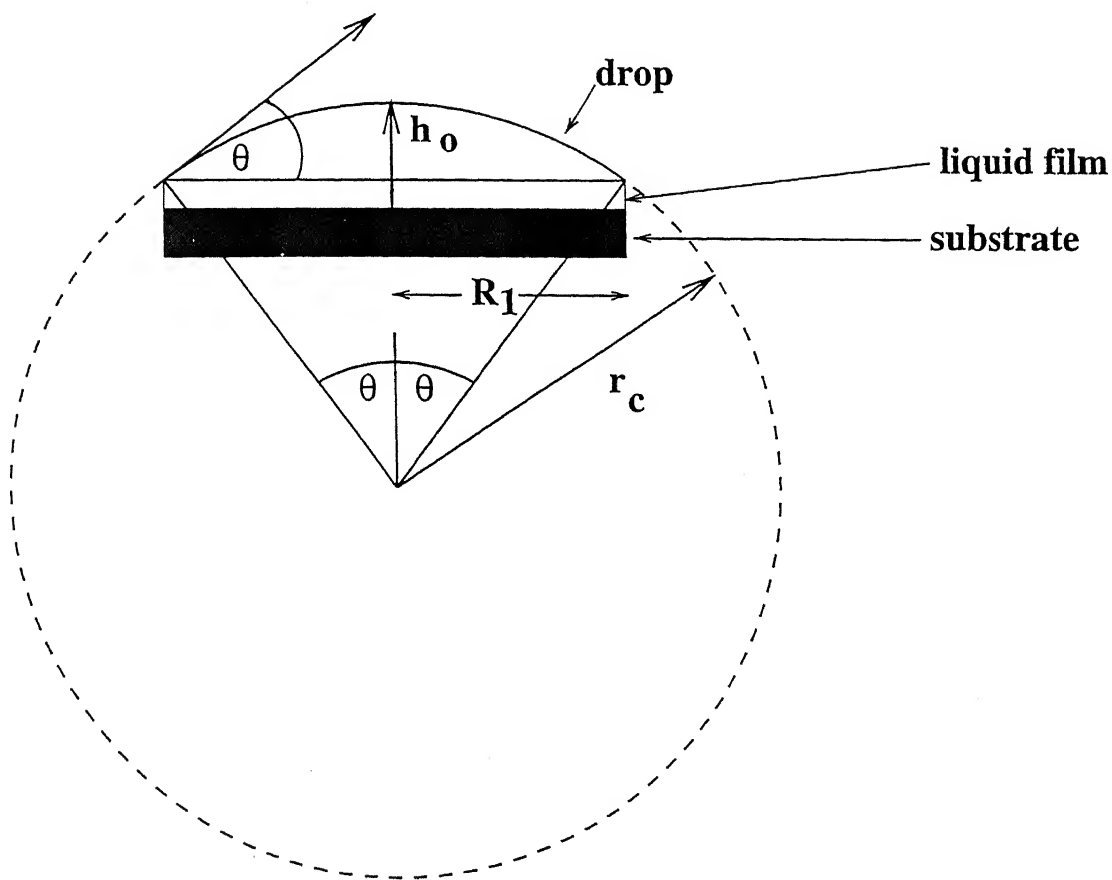
Fig. 4.3 Shape of critical nucleii for water for different values of S^{LW}. ($S^P = 0$, $p_v/p_o = 1.2$)

no.	S^{LW}
1	-5.0
2	-10.0
3	-15.0
4	-20.0
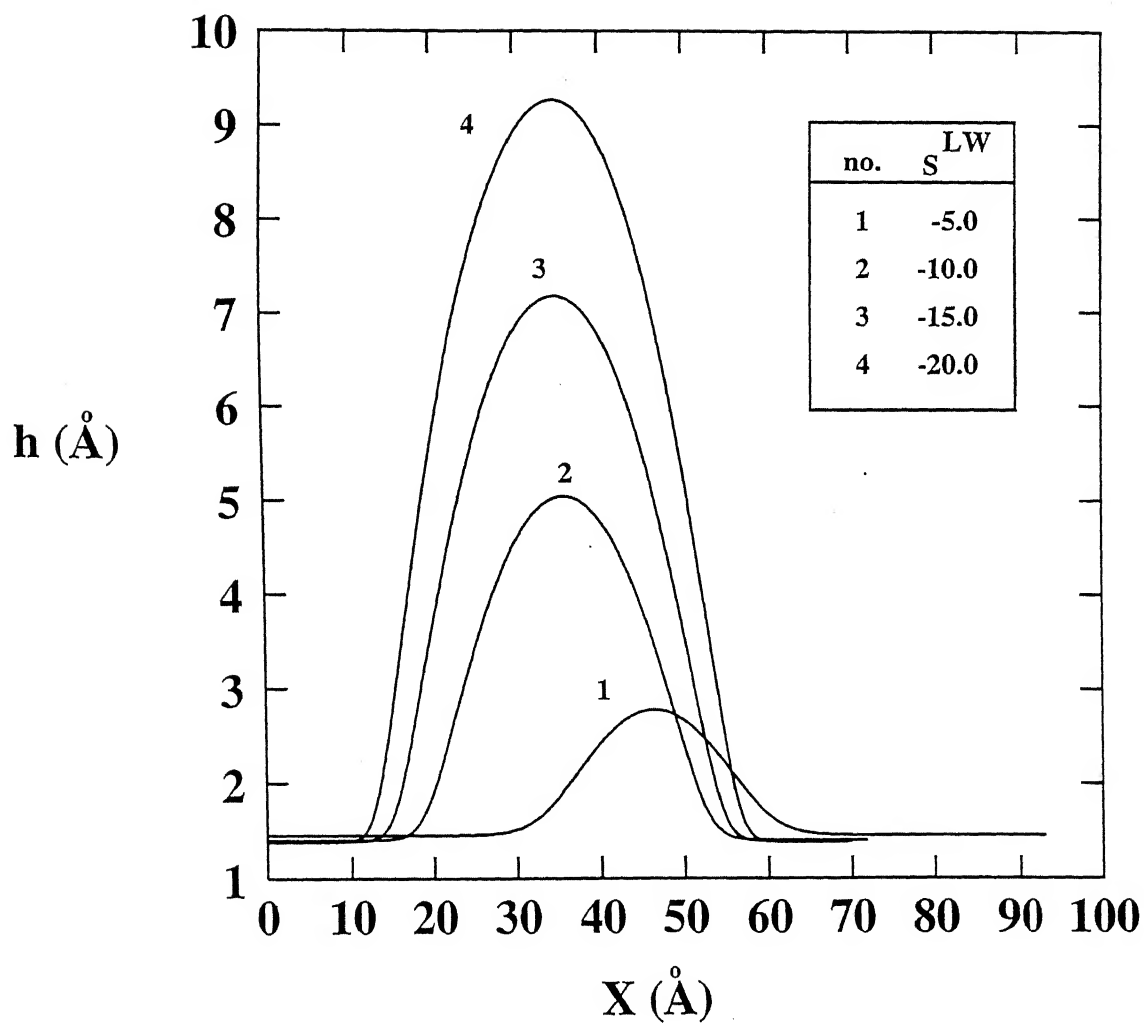
Fig. 4.4 Shape of critical nucleii for water for different values of p_v/p_o. ($S^P = 0$, $S^{LW} = -15$ dynes/cm)

Fig. 4.5 Shape of critical nucleii for water for different values of p_v/p_o. ($S^P = 0$, $S^{LW} = -15$ dynes/cm)

no.	$\frac{p_v}{p_o}$
6	1.6
7	1.7
8	1.8
9	1.9
10	2.0
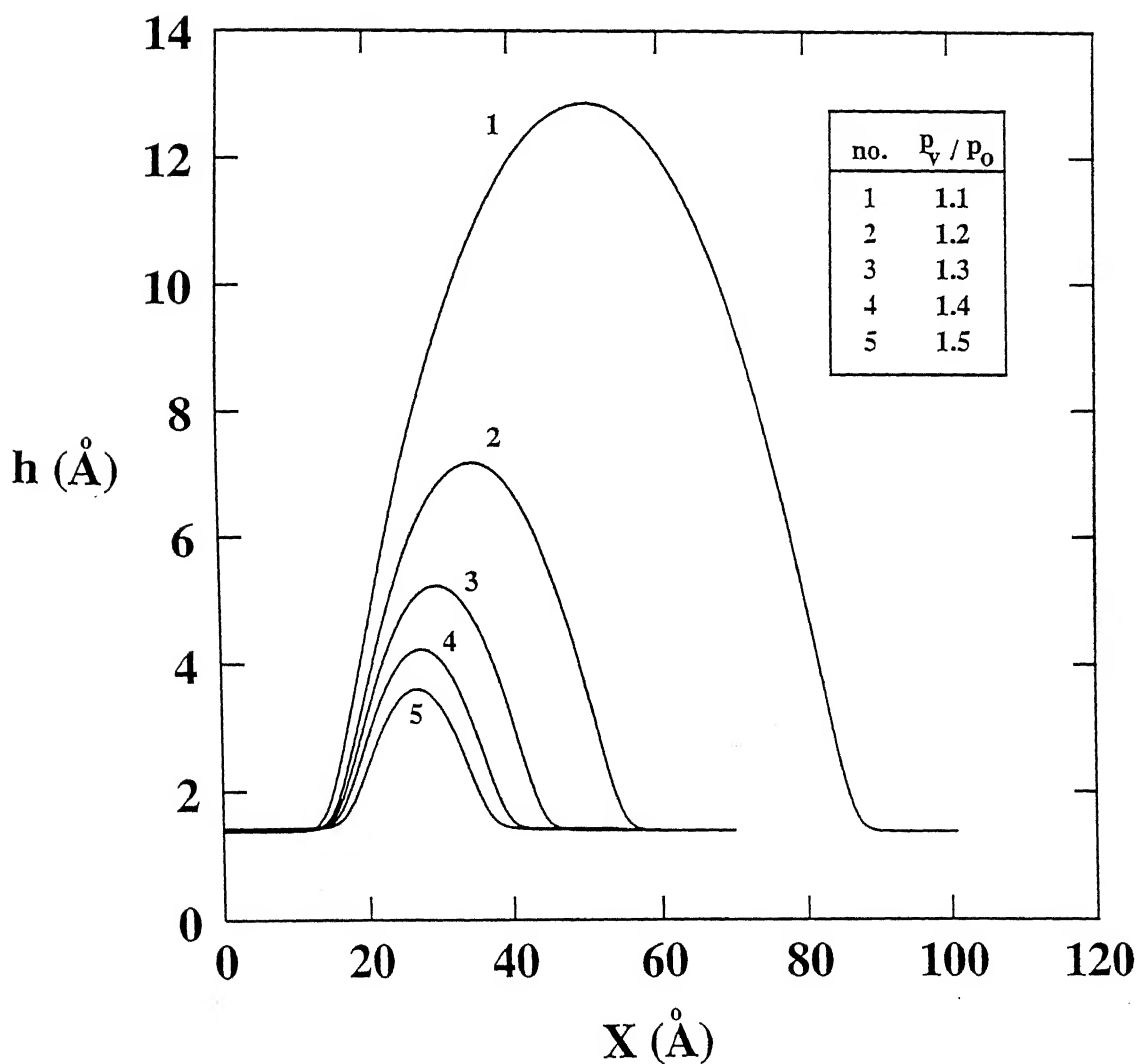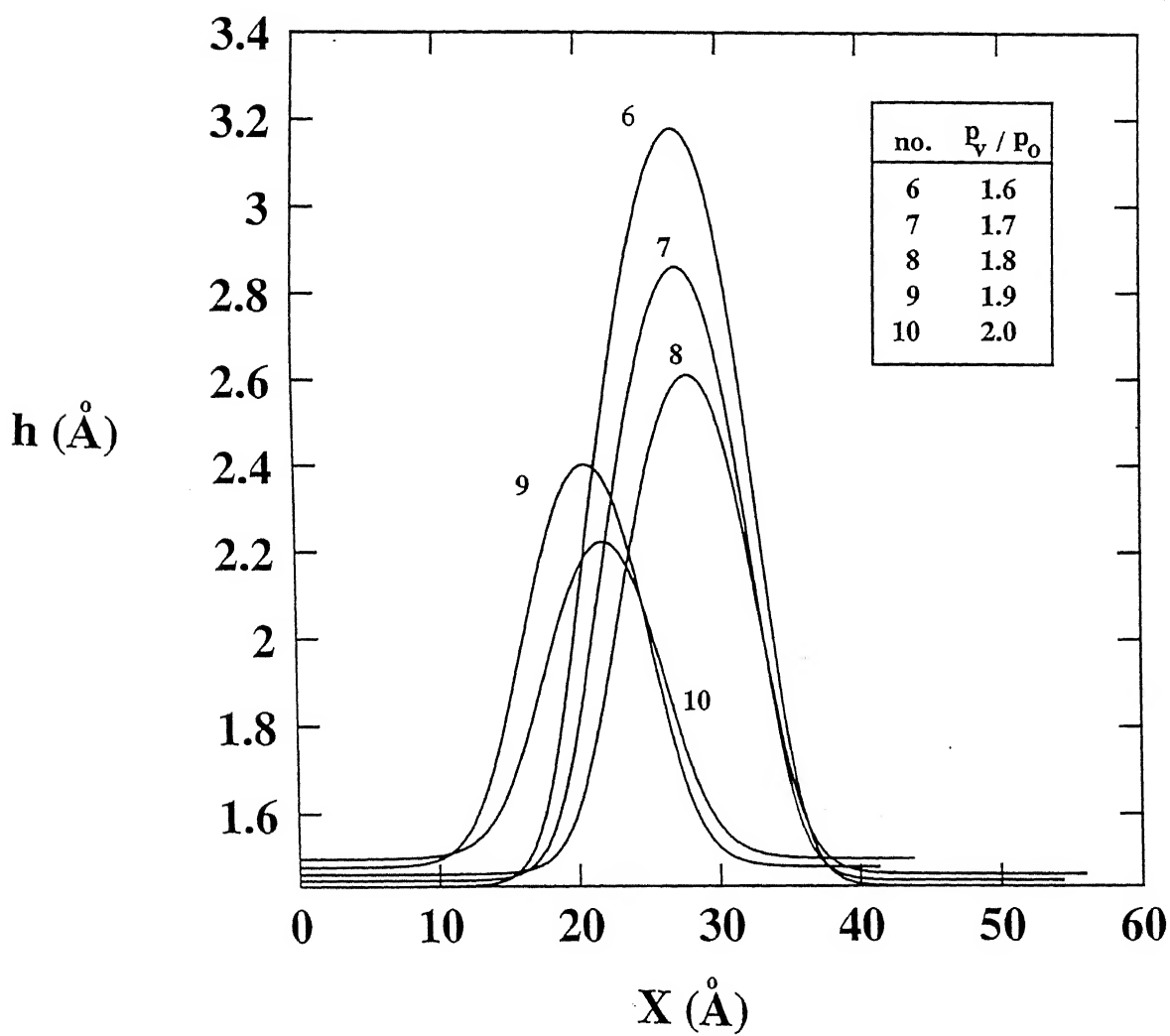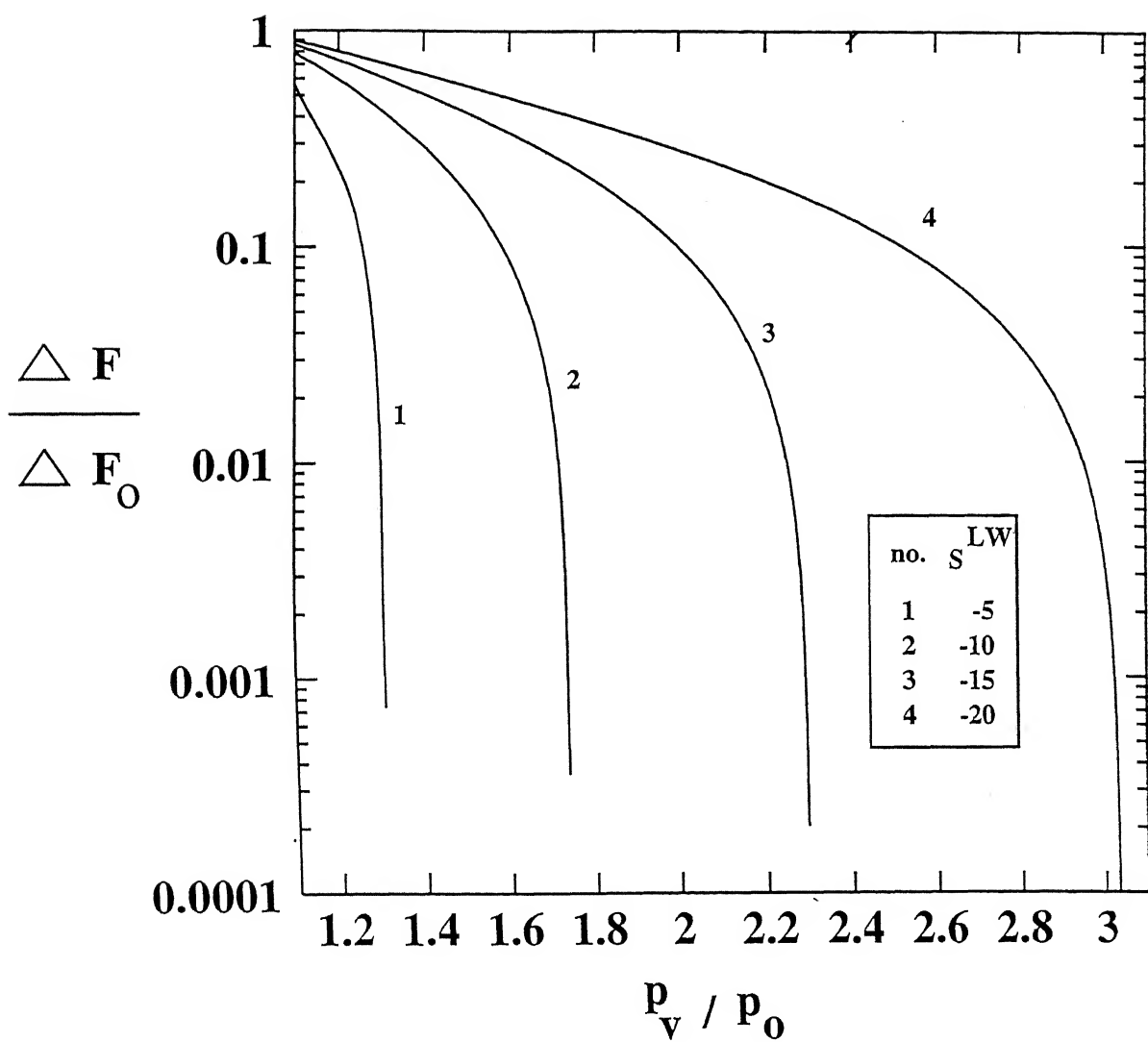
Fig. 4.6 Ratio of energy for critical nucleii of water from simulation and classical theory vs. p_v/p_o for different values of S^{LW}. ($S^P = 0$)

Fig. 4.7 Growth of a nucleus of water above critical nucleus. ($S^P = 0$, $S^{LW} = -15$ dynes/cm, $p_v/p_o = 1.2$, $C_1 = 0.071761$, $C_2 = 3.887 \times 10^{-2}$, $P = 0$)

no.	t (μs)	no.	t (μs)
1	0	7	2.7199
2	1.08	8	2.7204
3	1.80	9	2.88
4	2.16	10	3.60
5	2.52	11	5.40
6	2.7072		

Fig. 4.8 Decay of a nucleus of water below critical nucleus. ($S^P = 0$, $S^{LW} =$ -15 dynes/cm, $p_v/p_o = 1.2$, $C_1 = 0.05671$, $C_2 = 4.6374 \times 10^{-2}$, P = 0)

no.	t (μs)
1	0.000
2	0.180
3	0.360
4	0.540
5	0.576
6	0.612
7	0.900

Fig. 4.9 Ratio of energy for critical nucleii of Octane from simulation and classical theory vs. equilibrium contact angle for various values of p_v/p_o and surface tension. ($S^P = 0$) . . . .

no.	S.T.	p_v / p_o
1	10	3
3	20	3
5	30	3
7	50	3
2	10	2
4	20	2
6	30	2
8	50	2

$$\frac{\triangle F}{\triangle F_O}$$

θ
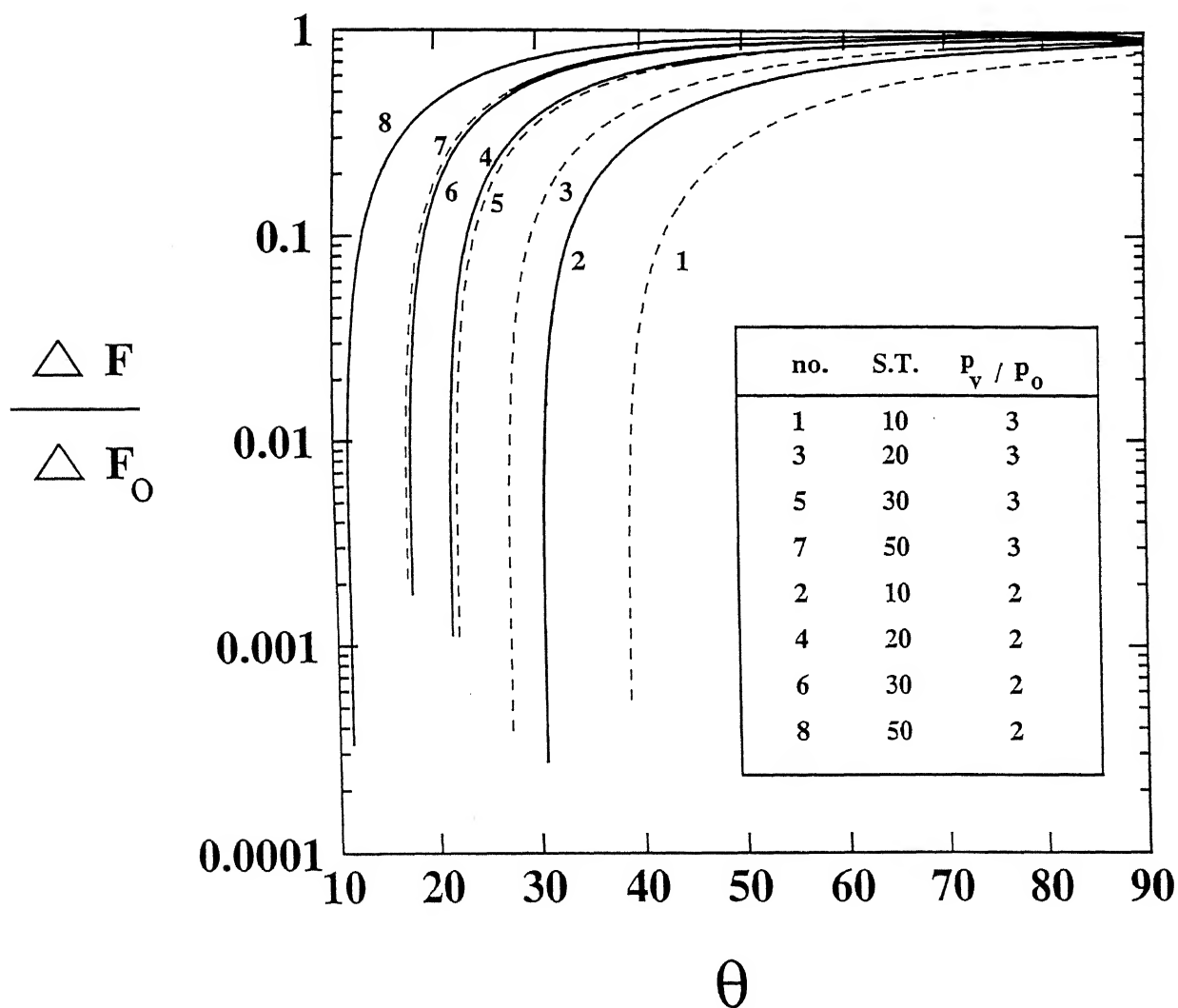
Fig. 4.10 Ratio of energy for critical nucleii of Octane from simulation and classical theory for higher range of p_v/p_o. ($S^P = 0$, $S^{LW} = -8$ dynes/cm.)
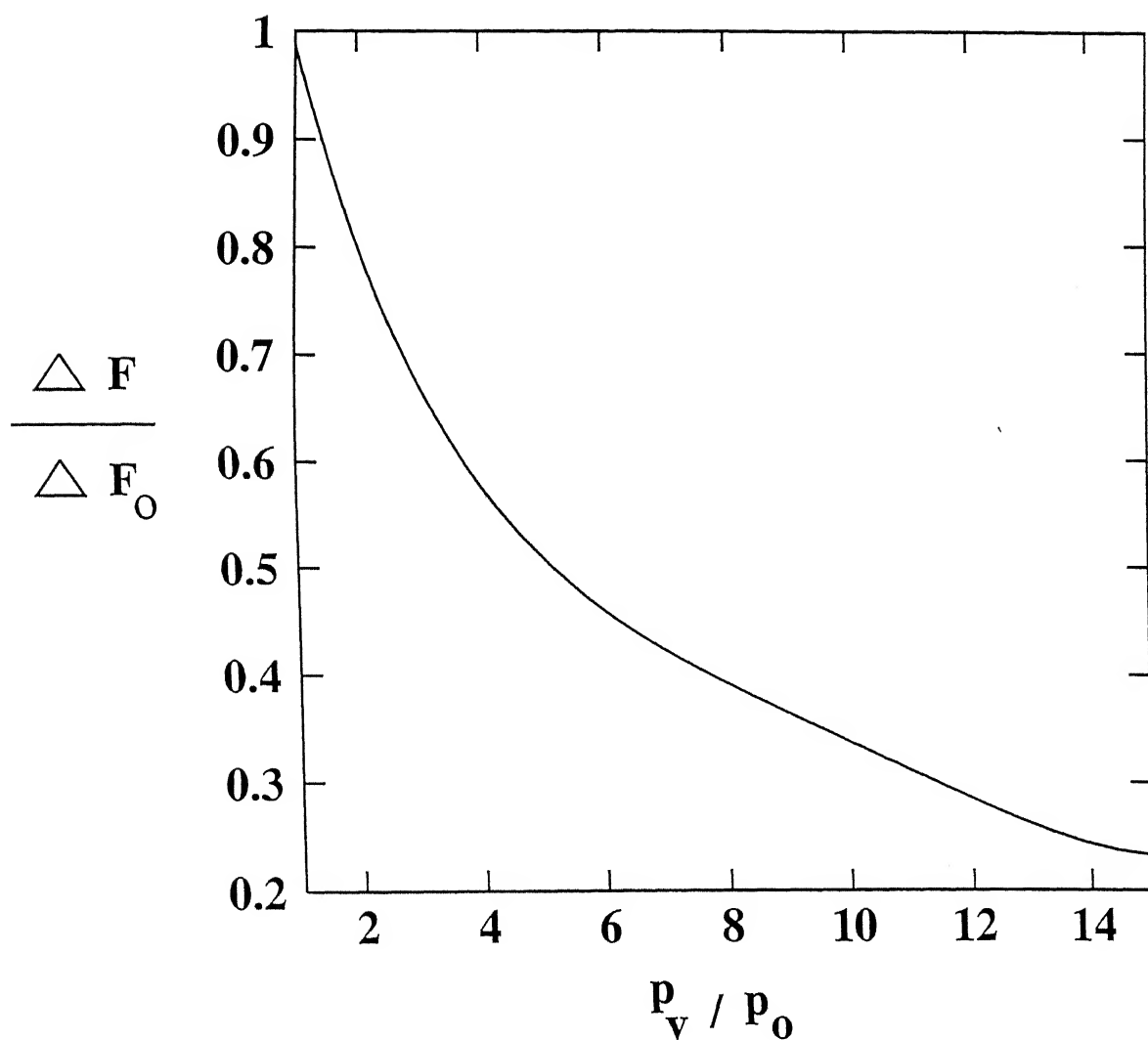
Fig. 4.11 Critical nucleii for Octane for different values of S^{LW}. ($S^P = 0$, $p_v/p_o = 1.2$)

no.	S^{LW}
1	-2
2	-4
3	-6
4	-8
5	-10
6	-12
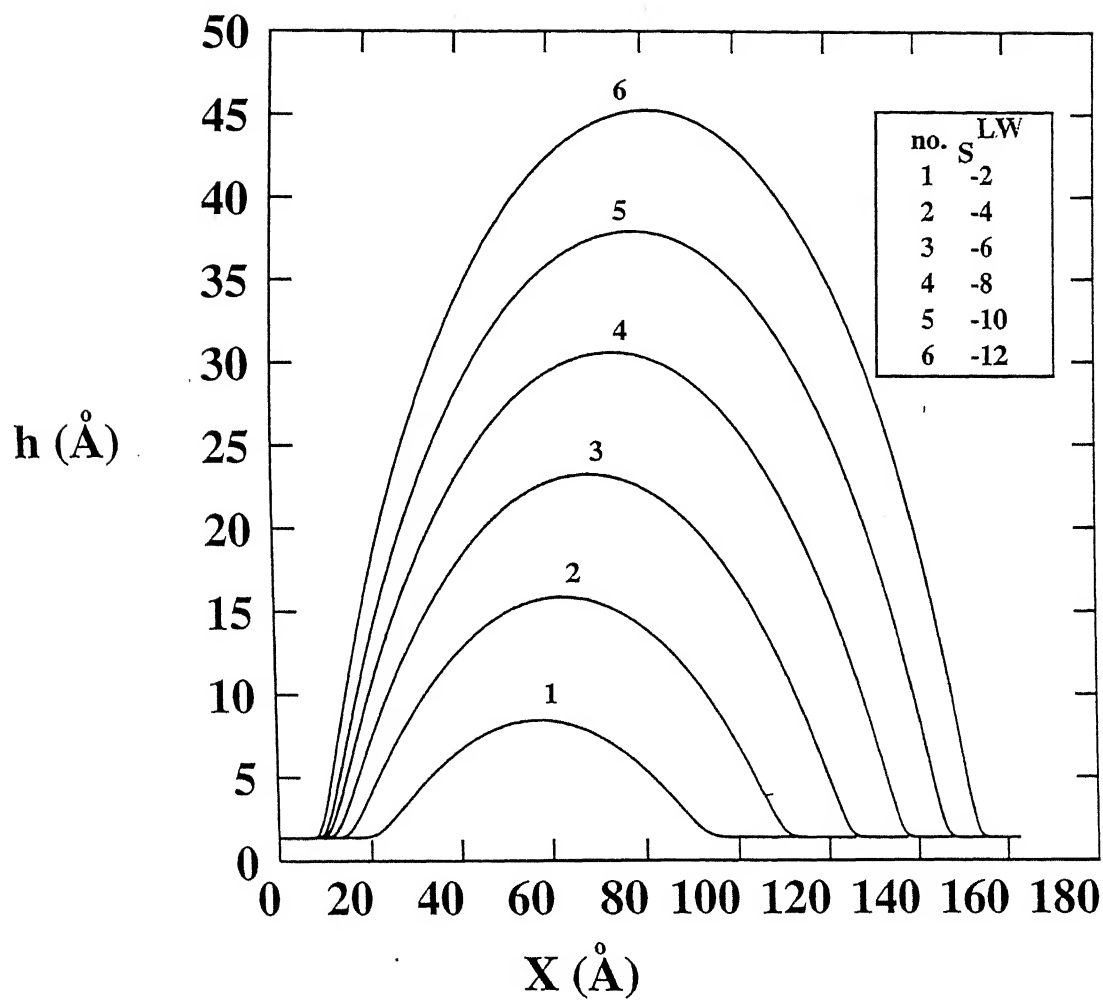
Fig. 4.12 Growth of a nucleus of Octane above critical nucleus. ($S^P = 0$, S^{LW} = -8 dynes/cm, $p_v/p_o = 1.2$, $C_1 = 29.28$, $C_2 = 0.24196 \times 10^{-2}$, P = 0)

no.	t (μ s)
1	0.00
2	0.14
3	0.70
4	1.40
5	2.10
6	2.38
7	2.52
8	2.80
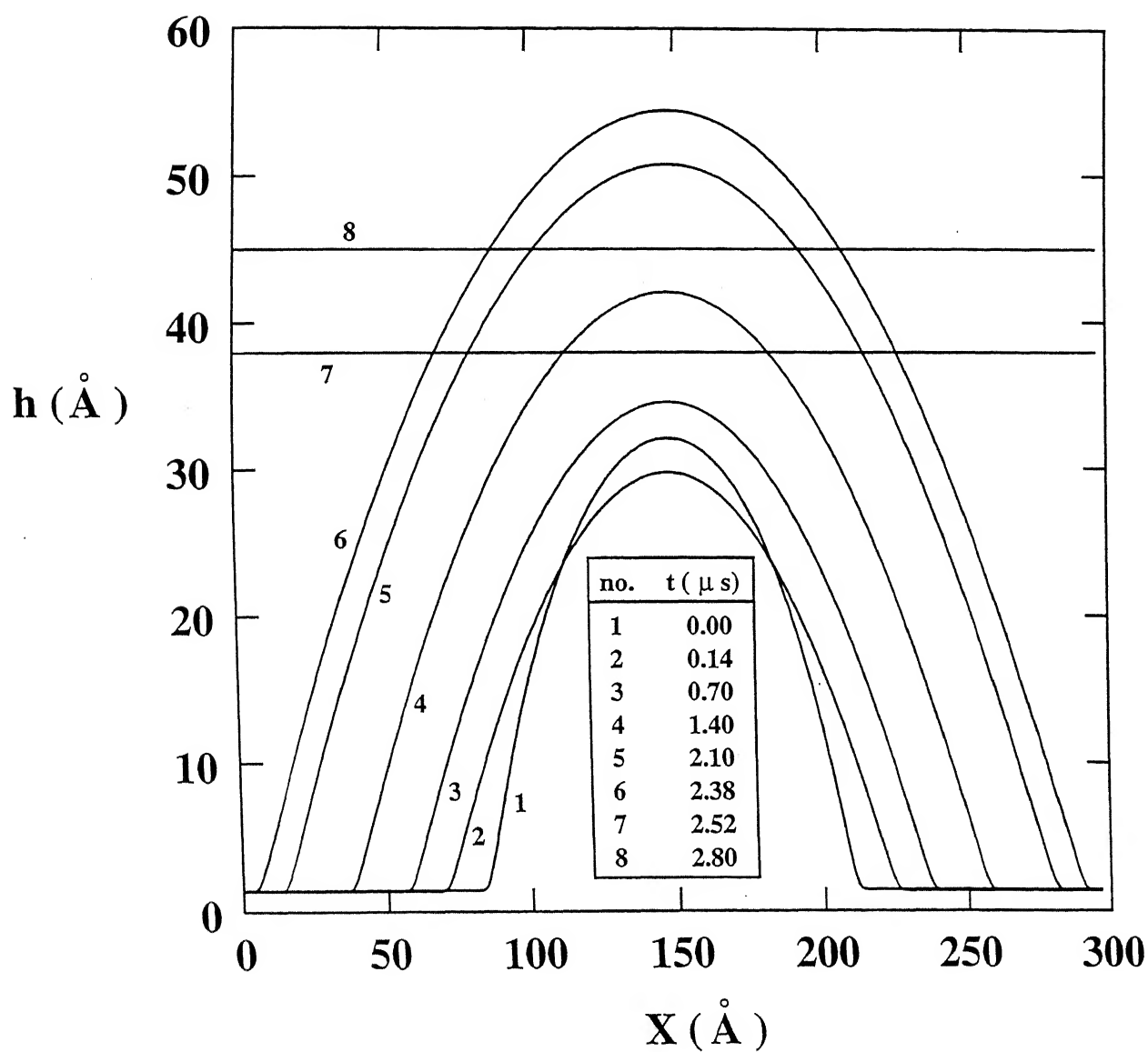
Fig. 4.13 Decay of a nucleus of Octane below critical nucleus. ($S^P = 0$, $S^{LW} = $ -8 dynes/cm, $p_v/p_o = 1.2$, $C_1 = 23.14$, $C_2 = 0.28868 \times 10^{-2}$, P = 0) .

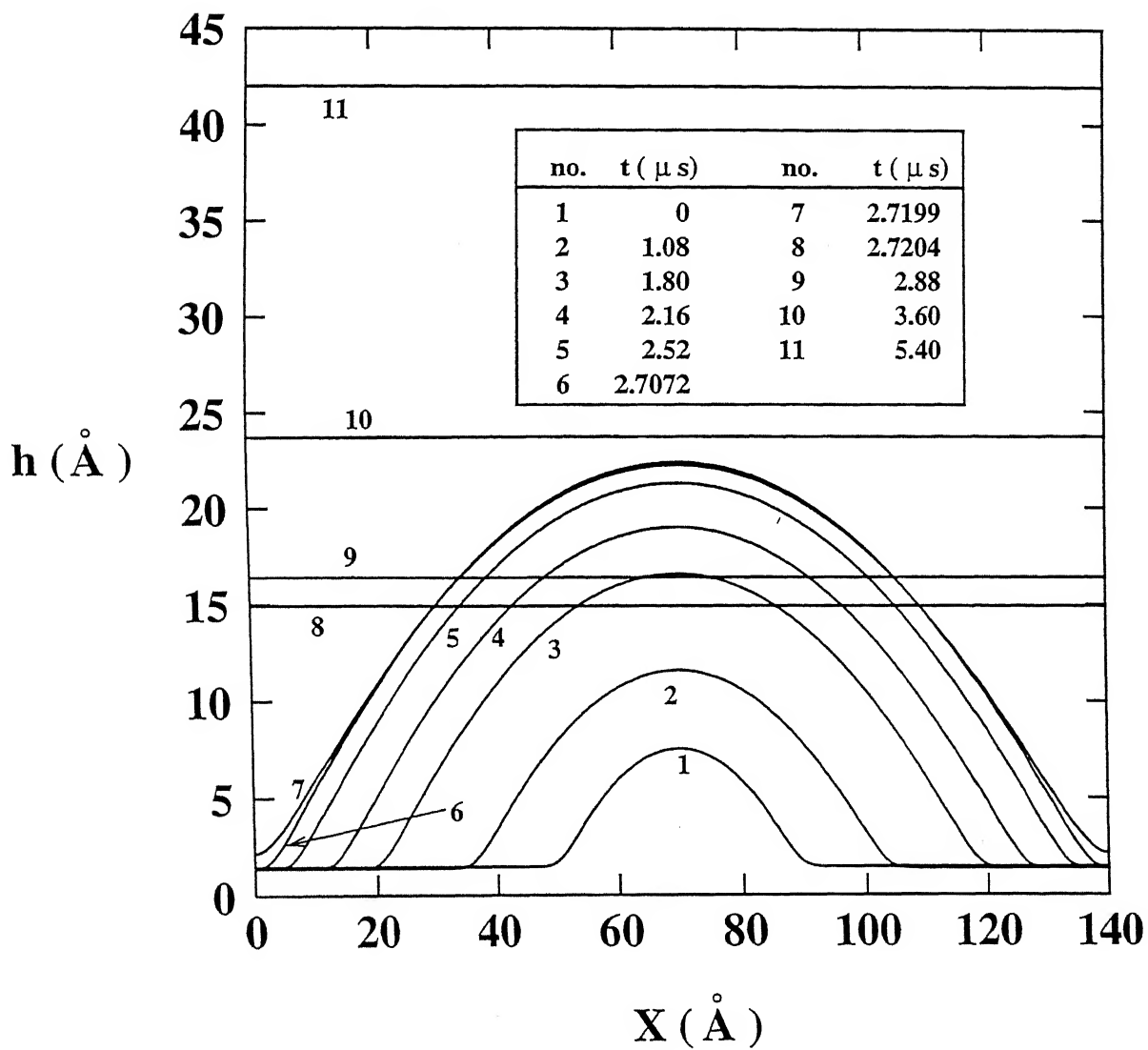| no.	t (μ s)
1	0.00
2	0.70
3	2.10
4	2.80
5	3.08
6	3.50
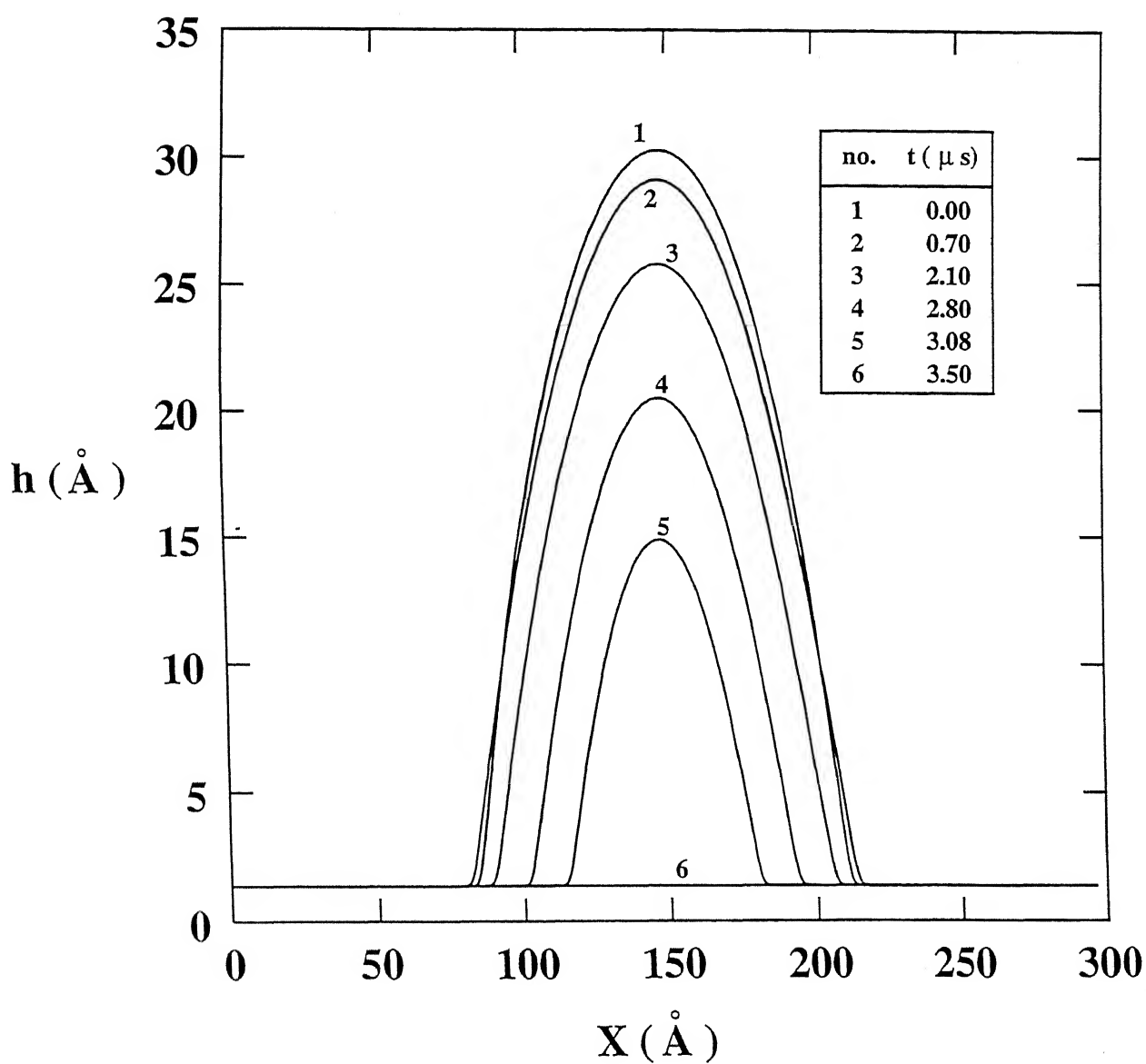
Fig. 4.14 Ratio of energy for critical nucleii of water from simulation and classical theory vs. equilibrium contact angle. ($S^{LW} = +15$ dynes/cm)

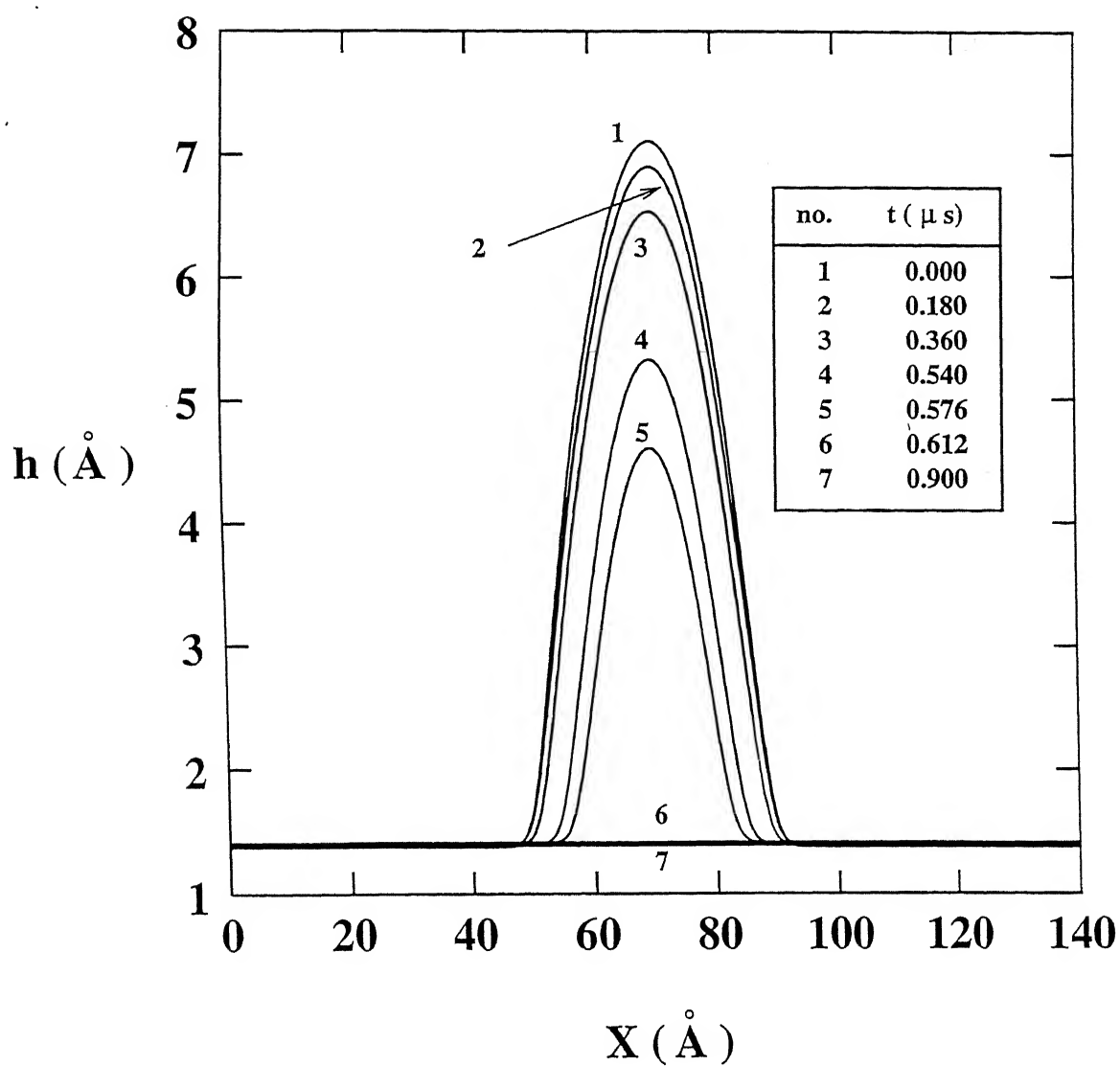| no.	p_v / p_o
1	1.2
2	1.5
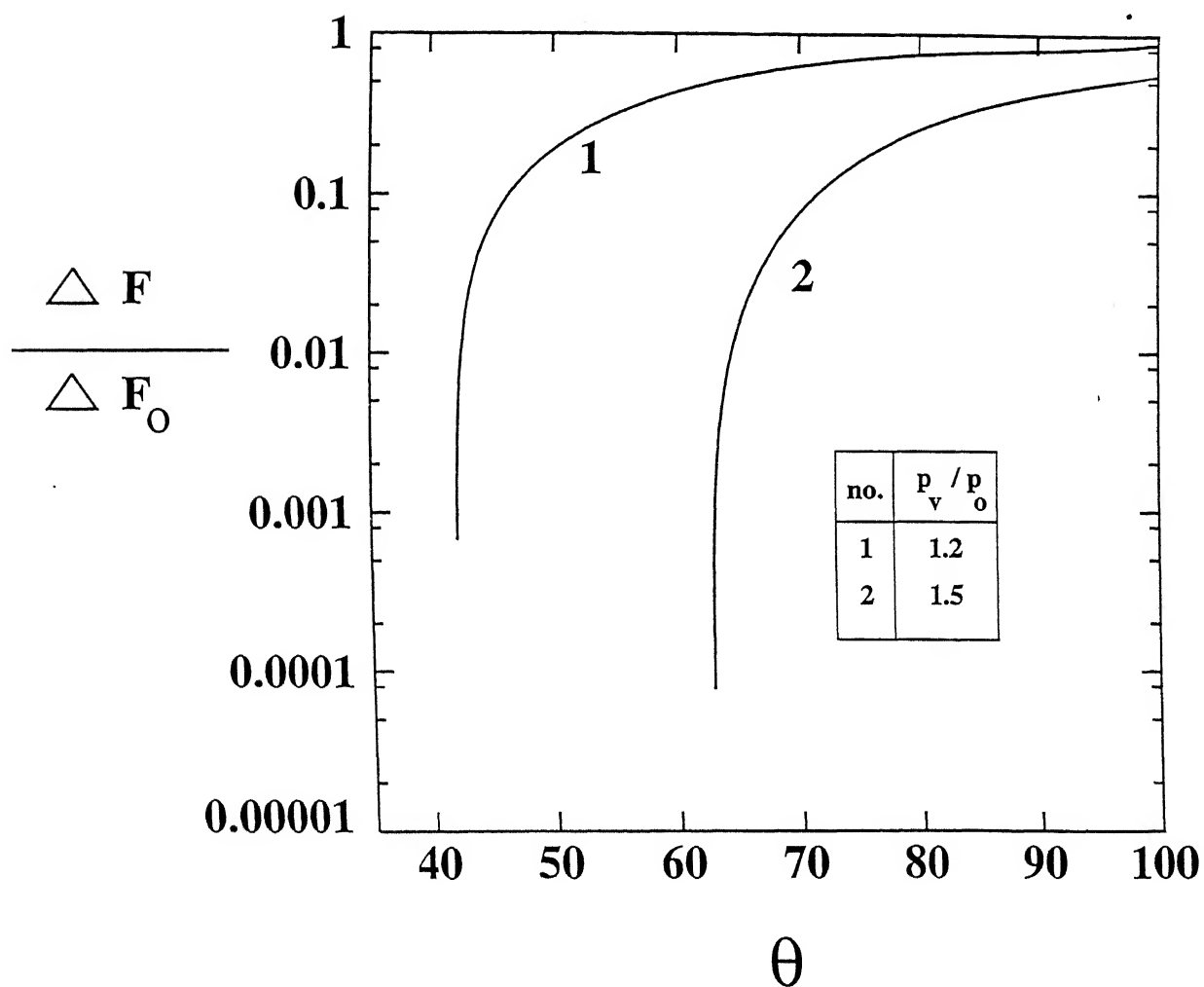
Fig. 4.15 Ratio of energy for critical nucleii of water from simulation and classical theory vs. equilibrium contact angle. $(S^{LW} = +20 \text{ dynes/cm})$

$$\frac{\triangle F}{\triangle F_O}$$

no.	P_v / P_0
1	1.2
2	1.5

θ
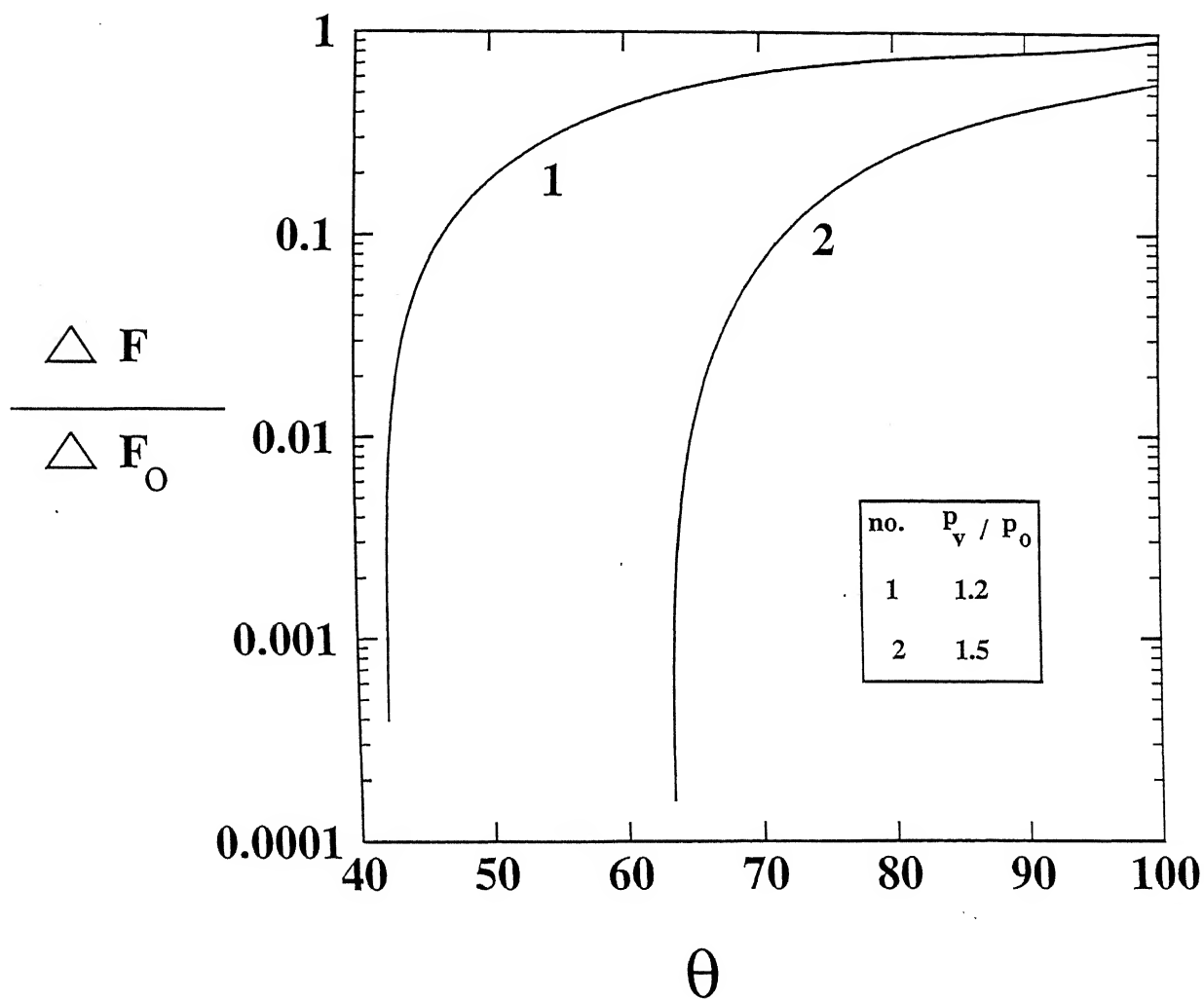
Fig. 4.16 Ratio of energy for critical nucleii of water from simulation and classical theory vs. p_v/p_o. ($S^{LW} = +15$ dynes/cm, $S^P = -50$ dynes/cm.)

Fig. 4.17 Growth of a nucleus of water above critical nucleus. ($S^P = $ -50 dynes/cm, $S^{LW} = +15$ dynes/cm, $p_v/p_o = 1.2$, $C_1 = 1.5970$, $C_2 = -0.3794 \times 10^{-2}$, P = 444.07)
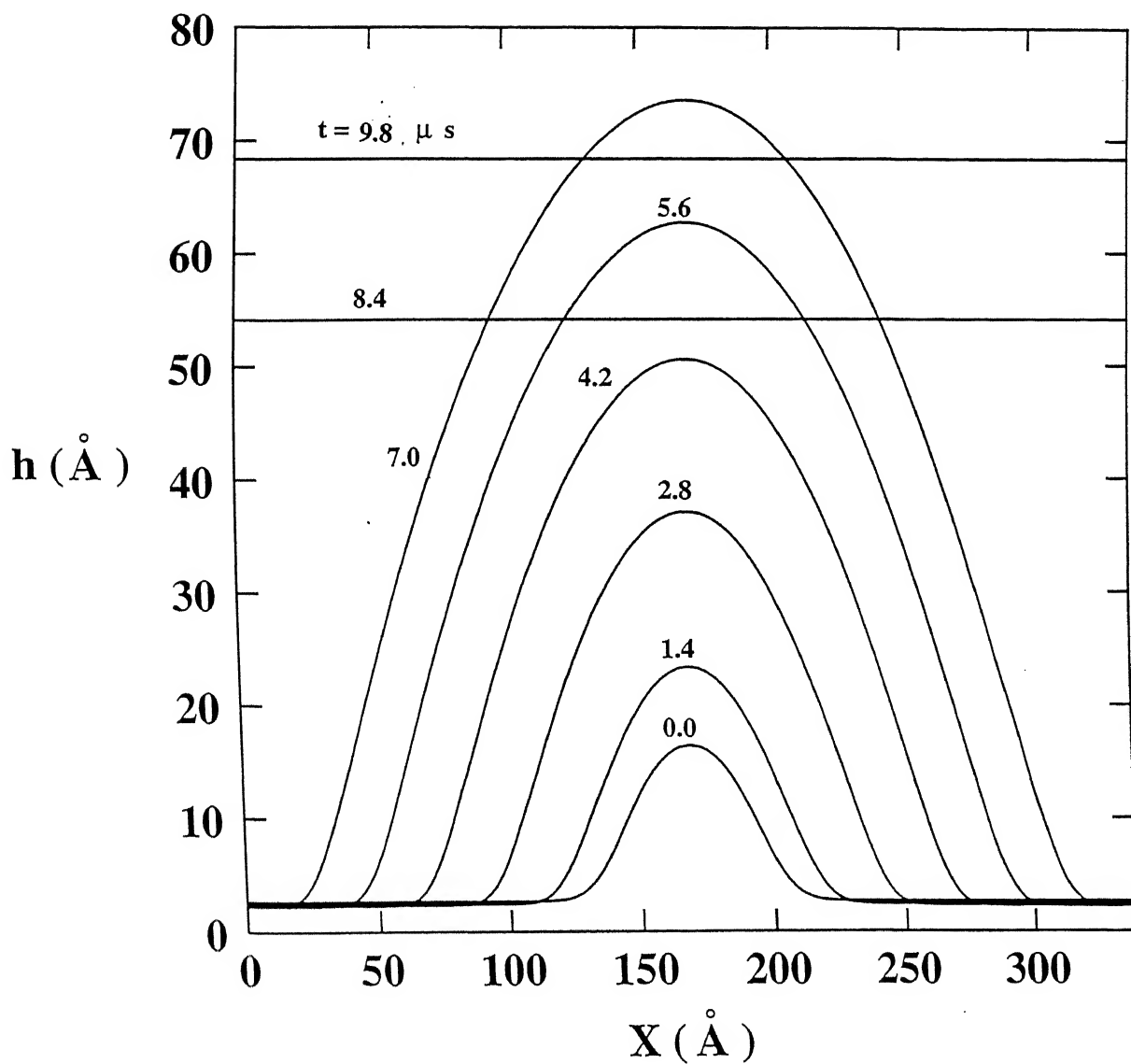
Fig. 4.18 Decay of a nucleus of water below critical nucleus. ($S^P = $ -50 dynes/cm, $S^{LW} = +15$ dynes/cm, $p_v/p_o = 1.2$, $C_1 = 1.0701$, $C_2 = -0.5122 \times 10^{-2}$, P = 297.57)
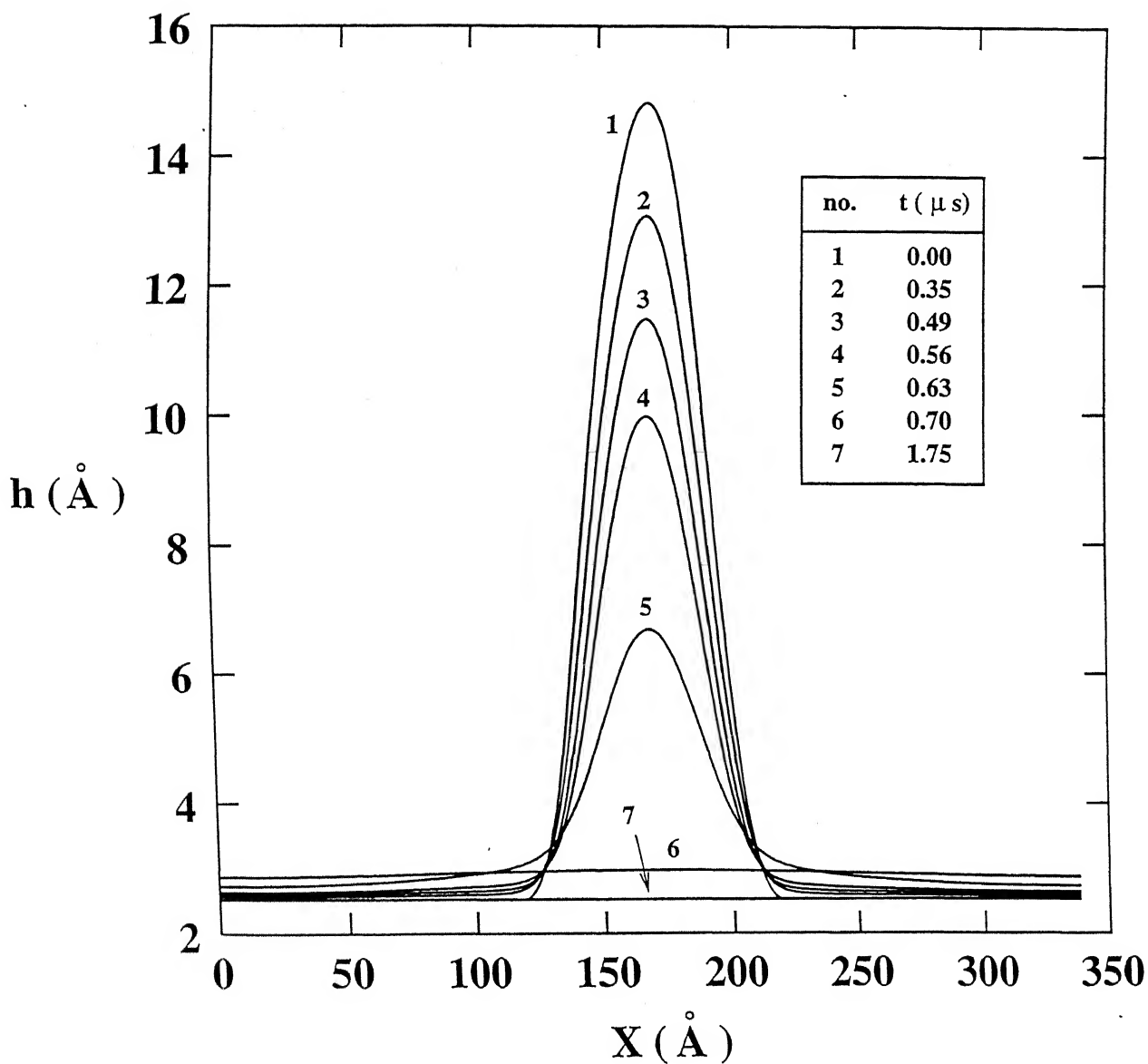
Table 4.1: Results for critical nucleii of Water ($S^{LW} = -15$ dynes/cm, $S^P = 0$).

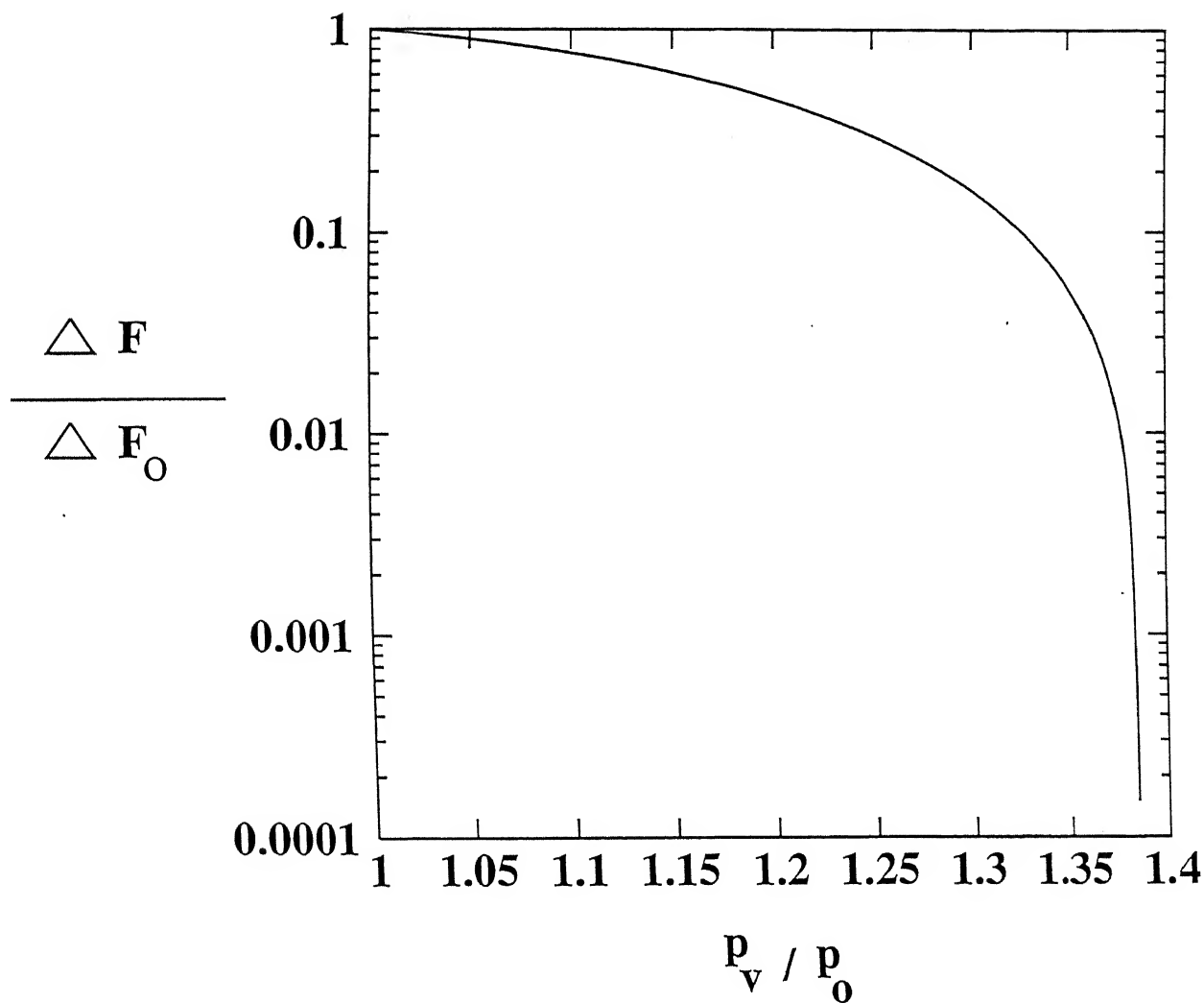| $\frac{p_v}{p_o}$	r_c (Å)	ΔG_{class} (ergs/cm)	h_e (Å)	h_o (Å)	$\Delta G_{critical}$ (ergs/cm)	θ_{max} (degrees)	$\frac{\Delta G_{crit}}{\Delta G_{class}}$
1.1	56.59	0.703×10^{-4}	1.379	12.858	0.606×10^{-5}	29.26	0.86
1.2	29.58	0.367×10^{-5}	1.390	7.179	0.268×10^{-5}	25.10	0.73
1.3	20.56	0.254×10^{-5}	1.400	5.233	0.156×10^{-5}	21.84	0.61
1.4	16.03	0.197×10^{-5}	1.412	4.231	0.101×10^{-5}	19.08	0.51
1.5	13.30	0.163×10^{-5}	1.423	3.609	0.681×10^{-6}	16.64	0.42
1.6	11.48	0.139×10^{-5}	1.436	3.180	0.470×10^{-6}	14.42	0.34
1.7	10.16	0.122×10^{-5}	1.449	2.861	0.325×10^{-6}	12.36	0.27
1.8	9.18	0.109×10^{-5}	1.464	2.610	0.221×10^{-6}	10.40	0.20
1.9	8.40	0.987×10^{-6}	1.480	2.403	0.145×10^{-6}	8.52	0.15
2.0	7.78	0.898×10^{-6}	1.499	2.225	0.890×10^{-7}	6.66	0.10
2.25	6.65	0.705×10^{-6}	1.577	1.816	0.708×10^{-8}	1.66	0.01
2.28	6.54	0.675×10^{-6}	1.599	1.748	0.228×10^{-8}	0.86	0.0034

Table 4.2: Results for critical nucleii of Octane. (S^{LW} = -8 dynes/cm, $S^P = 0$)

$\frac{p_v}{p_o}$	r_c (Å)	ΔG_{class} (ergs/cm)	h_e (Å)	h_o (Å)	$\Delta G_{critical}$ (ergs/cm)	θ_{max} (degrees)	$\frac{\Delta G_{crit}}{\Delta G_{class}}$
1.1	152.55	0.131×10^{-4}	1.370	57.309	0.128×10^{-4}	90.00	0.97
1.2	79.75	0.687×10^{-5}	1.372	30.557	0.653×10^{-5}	44.36	0.95
1.3	55.42	0.477×10^{-5}	1.374	21.599	0.443×10^{-5}	42.73	0.93
1.4	43.21	0.372×10^{-5}	1.376	17.094	0.337×10^{-5}	41.38	0.90
1.5	35.86	0.309×10^{-5}	1.378	14.373	0.273×10^{-5}	40.22	0.88
1.7	27.40	0.236×10^{-5}	1.381	11.231	0.199×10^{-5}	38.30	0.85
2.0	20.98	0.180×10^{-5}	1.385	8.827	0.144×10^{-5}	36.03	0.80
2.5	15.87	0.136×10^{-5}	1.391	6.897	0.991×10^{-6}	33.21	0.73
3.0	13.23	0.114×10^{-5}	1.396	5.888	0.762×10^{-6}	31.08	0.67
3.5	11.61	0.994×10^{-6}	1.400	5.258	0.621×10^{-6}	29.37	0.62
4.0	10.49	0.897×10^{-6}	1.404	4.821	0.525×10^{-6}	27.93	0.58
6.0	8.11	0.690×10^{-6}	1.418	3.874	0.323×10^{-6}	23.79	0.47
9.0	6.62	0.558×10^{-6}	1.433	3.254	0.200×10^{-6}	19.85	0.36
12.0	5.85	0.490×10^{-6}	1.446	2.924	0.140×10^{-6}	17.11	0.29
15.0	5.37	0.446×10^{-6}	1.457	2.709	0.104×10^{-6}	14.98	0.23

Table 4.3: Results for critical nucleii of Water (S^{LW} = 15dynes/cm, S^P = -50 dynes/cm)

$\frac{p_v}{p_o}$	r_c (Å)	ΔG_{class} (ergs/cm)	h_e (Å)	h_o (Å)	$\Delta G_{critical}$ (ergs/cm)	θ_{max} (degrees)	$\frac{\Delta G_{crit}}{\Delta G_{class}}$
1.03	182.47	0.846×10^{-4}	2.190	95.840	0.796×10^{-4}	52.05	0.94
1.10	56.59	0.261×10^{-4}	2.308	31.012	0.201×10^{-4}	39.08	0.77
1.15	38.59	0.177×10^{-4}	2.406	21.092	0.109×10^{-4}	31.72	0.61
1.20	29.58	0.135×10^{-4}	2.524	15.592	0.610×10^{-5}	25.11	0.45
1.25	24.17	0.108×10^{-4}	2.669	11.870	0.324×10^{-5}	18.90	0.30
1.30	20.56	0.898×10^{-5}	2.865	9.015	0.146×10^{-5}	12.81	0.16
1.34	18.43	0.777×10^{-5}	3.097	7.014	0.557×10^{-6}	7.72	0.07
1.35	17.97	0.748×10^{-5}	3.177	6.515	0.389×10^{-6}	6.36	0.052
1.38	16.75	0.646×10^{-5}	3.604	4.742	0.305×10^{-7}	1.50	0.0047

Bibliography

[1] Adamson, A.W., *Physical Chemistry of Surfaces,* Interscience Publishers, 2nd ed.

[2] C.S.Yih, *Proc. 2nd US Congr. Appl. Mech.* 628 (1967)

[3] T.B.Benjamin, *J. Fluid Mech.* **2**, 554 (1957)

[4] D.J.Benny, *J. Math. Phys.* **45**, 150 (1966)

[5] W.Atherton, G.M.Homsy, *Chem. Engg. Comm.* **2**, 57 (1976)

[6] A.Scheludko, *Adv. Colloid Interface Sci.* **1**, 391 (1967)

[7] A.Vrij, *Discuss. Faraday Soc.* **42**, 23 (1966)

[8] E.Ruckenstein, R.K.Jain, *J. Chem. Soc. Faraday Trans. II* **70**, 132 (1974)

[9] M.B.Williams, S.H.Davis, *J. Colloid Interface Sci.* **90**, 220 (1982)

[10] G.F.Teletzke, H.T.Davis, L.E.Scriven *Chem. Engg. Comm.* **55**, 41 (1987)

[11] A.Sharma, C.S.Kishore, S.Salaniwal, *Phys. Fluids ,* **7** (8), 1832 (1995).

[12] J.Wayner, *Colloids and Surfaces* **52**, 71 (1991).

[13] A.Sharma, *unpublished results.*

[14] K.Hickman, *Ind. Engg. Chem.* **44**, 1892 (1952)

[15] H.J.Palmer, J.C.Maheshri, *Int. J. Heat Mass Transfer* **24**, 117 (1981)

[16] S.G.Bankoff, *Int. J. Heat Mass Transfer* **14**, 337 (1971)

[17] J.P.Burelbach, S.G.Bankoff, S.H.Davis, *J. Fluid Mech.* **195,** 463 (1988)

[18] A.Sharma, E.Ruckenstein, *PCH Physico Chemical Hydrodynamics* **10,** 675 (1988)

[19] A.Sharma, E.Ruckenstein, *J. Colloid Interface Sci.* **113,** 456 (1986)

[20] A.Sharma, E.Ruckenstein, *Langmuir* **2,** 480 (1986)

[21] S.Salaniwal, *M. Tech. Thesis* I.I.T. Kanpur, 1995

[22] A.Sharma, *Langmuir* **9,** 3580 (1993).

[23] A.Sharma, A.T.Jameel, *J. Colloids Interface Sci.* **164,** 416 (1994).

[24] B.R.Bird, W.E.Stewart, E.N.Lightfoot, *Transport Phenomena*

[25] A.Sharma, A.T.Jameel, *J. Colloid Interface Sci.* **161,** 190 (1993)

[26] A.Sharma, A.T.Jameel, *J. Chem. Soc. Faraday Trans. II* **90,** 625 (1994)

[27] R. Khanna, *M. Tech. Thesis* I.I.T. Kanpur, 1992

[28] K.R.Guruvayurappan, *M. Tech. Thesis* I.I.T. Kanpur, 1994

[29] Hunter, R.J., *Foundations of Colloidal Sci.*

[30] Hiemenz, Z., *Principles of Colloid and Surface Chemistry* Marcel Dekker, Inc., 2nd ed.